Heat Transfer in Thermoelectric Materials and Devices

Heat Transfer in Thermoelectric Materials and Devices

Zhiting Tian

Sangyeop Lee

Gang Chen
e-mail: gchen2@mit.edu

Department of Mechanical Engineering,
Massachusetts Institute of Technology,
Cambridge, MA 02139

Solid-state thermoelectric devices are currently used in applications ranging from thermocouple sensors to power generators in space missions, to portable air-conditioners and refrigerators. With the ever-rising demand throughout the world for energy consumption and CO_2 reduction, thermoelectric energy conversion has been receiving intensified attention as a potential candidate for waste-heat harvesting as well as for power generation from renewable sources. Efficient thermoelectric energy conversion critically depends on the performance of thermoelectric materials and devices. In this review, we discuss heat transfer in thermoelectric materials and devices, especially phonon engineering to reduce the lattice thermal conductivity of thermoelectric materials, which requires a fundamental understanding of nanoscale heat conduction physics. [DOI: 10.1115/1.4023585]

Keywords: heat transfer, thermoelectric, nanostructuring, phonon transport, electron transport, thermal conductivity

1 Introduction

Thermoelectric effects have long been known since the Seebeck effect and the Peltier effect were discovered in the 1800s [1]. The Seebeck effect occurs when a temperature gradient over a conductor or semiconductor generates a voltage. This effect is the basis of thermocouples and can be applied to thermal-to-electrical energy generation. The inverse process, in which an electrical current creates cooling or heat pumping at the junction between two dissimilar materials, corresponds to the Peltier effect. The 1950s saw extensive research and applications on Peltier refrigerators following the emergence of semiconductors and their alloys as thermoelectric materials [1]. However, the research efforts waned as the efficiency of solid-state refrigerators could not compete with mechanical compression cycles. Starting in the 1990s, interest in thermoelectrics renewed because of increased global energy demand and global warming caused by excessive CO_2 emissions [1].

The maximum efficiency of a thermoelectric material for both thermoelectric power generation and cooling is determined by the dimensionless figure-of-merit ZT,

$$ZT = \frac{S^2\sigma}{\kappa}T \tag{1}$$

where S is the Seebeck coefficient, σ is the electrical conductivity, $S^2\sigma$ is the power factor, and $\kappa = \kappa_p + \kappa_e$ is the thermal conductivity composed of lattice, i.e., phononic, thermal conductivity κ_p, and electronic thermal conductivity κ_e. The Seebeck coefficient is voltage generated per degree of temperature difference over a material. Fundamentally, it is a measure of the average entropy carried by a charge in the material. A large power factor means electrons are efficient in the heat-electricity conversion, while a small thermal conductivity is required to maintain a large temperature gradient and reduce conductive heat losses. Achieving high ZT values requires a material simultaneously possessing a high Seebeck coefficient and a high electrical conductivity but maintaining a low thermal conductivity, which is challenging as these requirements are often contradictory to each other [2]. The improvements in ZT have been realized in large part due to modification of thermal transport properties, and thus our review focuses on understanding the physical mechanisms giving rise to these changes in thermal properties. Thermoelectric devices often consist of many pairs of p-type and n-type semiconductors pellets connected electrically in series and thermally in parallel. One needs to optimize the geometry of p-type and n-type legs and use materials with large ZT values to maximize efficiency. True ZT values of a pair are dependent on a combination of the properties of the two legs. For simplicity in the materials search, however, we usually use ZT for individual materials as defined in Eq. (1) to gauge their potential for thermoelectric applications.

Recent years have witnessed impressive progress in thermoelectric materials, stimulated by new ideas in bulk materials [3,4] and nanostructures [5,6]. There have been many reviews [2,7–22] covering different aspects of thermoelectrics, including bulk thermoelectric materials [11,12], individual nanostructures [13,14], and bulk nanostructures [8–10]. We would like to emphasize that even with current materials, there is space for innovation and development of thermoelectric technology to take advantage of their solid-state nature, scalability, silent operation, and environmental friendliness. Often times, it is poor heat transfer design that prevents achieving the ideal efficiency. The heat transfer community can play an active role in advancing thermoelectric technology by contributing to the understanding of heat transfer physics in materials, and device and system innovation. Our review will emphasize heat transfer physics in materials and device level heat transfer issues. We will start with a brief summary of materials status (Sec. 2), followed by a discussion on heat conduction mechanisms in bulk materials (Sec. 3), and strategies to reduce thermal conductivity in bulk materials (Sec. 4) and via nanostructures (Sec. 5). Heat transfer issues at device and system levels will be presented in Sec. 6.

2 Progress in Thermoelectric Materials

Classical thermoelectric materials are based on Bi_2Te_3 and its alloys with Bi_2Se_3 and Sb_2Te_3, PbTe and its alloys with PbSe and SnTe, and SiGe alloys. These materials were identified in the 1950s [23–25]. Bi_2Te_3 and PbTe contain heavy elements in the periodic table, which lead to small phonon group velocity and low thermal conductivity. Such heavy elements usually have small bandgaps and large mobility [11]. SiGe alloys, however, have large bandgaps and relatively light masses. Ioffe et al. [26] suggested that by alloying, thermal conductivity can be reduced, and this strategy has proved to be effective in all thermoelectric materials. These three materials cover quite a wide range of temperatures. Currently, Peltier cooling devices on the market are almost exclusively based on Bi_2Te_3. Power generation used in NASA

Manuscript received October 17, 2012; final manuscript received January 15, 2013; published online May 16, 2013. Assoc. Editor: Leslie Phinney.

space missions relied mostly on SiGe alloys because they have a large bandgap such that the hot side can be operated at high temperatures (1300 K) and the cold side can also be operated at elevated temperatures to reduce the size of radiators.

Between the 1950s and the 1990s, progress in *ZT* improvements was slow. However, in the 1990s, interest in thermoelectric energy conversion was renewed, first in potential refrigeration applications and subsequently more in power generation. New scientific ideas [5,6,27,28], together with investments from the US government and other governments all over the world, led to impressive progress in materials, as we will briefly summarize below.

2.1 Bulk Thermoelectric Materials. Alloying remains an active research area. Bi_2Te_3 alloys, p-type $Bi_xSb_{2-x}Te_3$ and n-type $Bi_2Te_{1-x}Se_x$, have *ZT* values around 1 [12] and have been in commercial thermoelectric cooling modules near room temperature and power generation modules for temperatures up to 500 K. Group IV tellurides are typical thermoelectric materials for 600–800 K range. PbTe alloys, such as p-type $PbTe_{1-x}Se_x$ and n-type $Pb_{1-x}Sn_xTe$, were reported to exhibit $ZT \sim 1$ [1,7] with over 40% thermal conductivity reduction from that of PbTe at 300 K. Most recent efforts on p-type $PbTe_{1-x}Se_x$ were able to achieve $ZT \sim 1.6$–1.8 [11,29,30], along with band engineering to optimize the power factor, although lately a record high *ZT* of 2.2 is reported by concurrently increasing the electron power factor and reducing the phonon thermal conductivity [31]. Another notable material $(AgSbTe_2)_{1-x}(GeTe)_x$, known as TAGS, has shown $ZT > 1$ for both p-type and n-type, although only p-type with $ZT \sim 1.2$ has been successfully used in long-term power generators [2,11]. SiGe alloys are candidates for high temperature applications because their peak *ZT* values are located at >900 K, and they exhibit long reliability. SiGe alloys possess $ZT \sim 1$ for n-type and $ZT \sim 0.6$ for p-type [11], but recent efforts through nanostructuring has led to peak *ZT* of 1.3 for n-type [32] and 0.9–1 for p-type [33].

Ideal thermoelectric materials are sometimes summarized as phonon-glass electron-crystals (PGEC). The terminology of PGEC was first put forward by Slack [3] to describe that ideal thermoelectric materials should achieve glass-like lattice thermal conductivity but crystal-like electron transport. One new idea Slack proposed is to reduce phonon thermal conductivity by the so called "phonon rattlers." By introducing guest atoms or molecules into the voids of an open cage structure, the atomic rattlers interact with a broad spectrum of phonons and form phonon scattering centers. The lattice thermal conductivity can thus be substantially reduced. Two representative classes of materials that have received attention are skutterudites and clathrates.

Skutterudites are actively pursued by many groups for potential power generation applications in the 500–900 K temperature range. Skutterudites' crystal formula can be written in MX_3 where M is Co, Rh, or Ir and X is P, As, or Sb. The key feature is large empty space that can be filled with different elements such as rare-earth, alkaline-earth, or other heavy atoms [34–37], which led to thermal conductivity reduction. Recently, the double-filled n-type $Ba_xYb_yCo_4Sb_{12}$ was observed to have an order of magnitude reduction in the lattice thermal conductivity (~0.9 W/mK at room temperature) compared to $CoSb_3$ and was shown to have a $ZT \sim 1.4$ [38] while triple-filled n-type $Ba_xLa_yYb_zCo_4Sb_{12}$ possesses even lower lattice thermal conductivity (~0.2 W/mK) and $ZT \sim 1.7$ [39]. Progress with p-type skutterudites has been slower since filling tends to drive skutterudites strong n-type and the best p-type skutterudites have $ZT \sim 1$ [40].

Clathrates are another class of compound, which has open structures to host loosely bound guest atoms. Clathrates typically have a large number of atoms in the unit cell and generally have low thermal conductivity (~1 W/mK at room temperature) comparable to that of amorphous germanium [24]. Two types of clathrates exist, with Type I more common. Type I clathrates can be represented by $X_2Y_6E_{46}$ where X and Y are guest atoms encapsulated in two different cages and E is Si, Ge, or Sn. A highest $ZT \sim 1.4$ has been reported for n-type single crystal $Ba_8Ga_{16}Ge_{30}$ [41], while fairly low $ZT \sim 0.6$ was observed for p-type $Ba_8Ga_{16}Al_3Ge_{27}$ [42].

Another idea to approach PGEC is to look for more complex structures, either large unit cells or complex compositions. Complex crystal structures have more optical phonon branches with low group velocities and, consequently, low thermal conductivities. Complex structures are known to have exceptionally low lattice thermal conductivities [12], such as β-Zn_4Sb_3 (0.65 W/mK [43]), the Zintl phase $Yb_{14}MnSb_{11}$ (0.4 W/mK [44]), and thallium chalcogenides ($Tl_9BiTe_6 \sim 0.39$ W/mK [45], $Ag_9TlTe_5 \sim 0.23$ W/mK [46]). Rare-earth chalcogenides [11] with Th_3P_4 structure have a large number of random vacancies and relatively low thermal conductivity ($La_{3-x}Te_4 \sim 0.5$ W/mK [12]).

Half-Heusler compounds possess a cubic structure consisting of three interpenetrating FCC sublattices and one vacant sublattice, with high thermal stability and environmental friendliness. They exhibit promising power factors with proper doping. Uher et al. [47] unveiled the unusual electron transport properties related to a semimetal-semiconductor transition at low temperatures and the presence of heavy electrons at high temperatures. A remarkably high power factor was observed in n-type alloys. However, half-Heusler compounds typically have a relatively high lattice thermal conductivity of ~10 W/mK. By alloying and nanostructuring, the lattice thermal conductivity can be reduced to ~3 W/mK and lead to $ZT \sim 1$ in p-type $Zr_{1-x}Ti_xCoSb_{0.8}Sn_{0.2}$ [48] and n-type $Hf_{1-x}Zr_xNiSb_{0.99}Sn_{0.01}$ [49]. Later it was also demonstrated that a larger mass difference between Hf and Ti than between Zr and Ti led to more severe thermal conductivity reduction in $Hf_{1-x}Ti_xCoSb_{0.8}Sn_{0.2}$ [50](~2 W/mK) than$Zr_{1-x}Ti_xCoSb_{0.8}Sn_{0.2}$ [48].

Oxides, a relative newcomer to thermoelectric fields, are potentially stable and chemically inert for high-temperature applications. Oxides were believed to be poor thermoelectric materials because of the low carrier mobility arising from the weak orbital overlap and localized electrons until the discoveries of good p-type thermoelectric properties in layered cobaltites $NaCo_2O_4$ [51] (1997), $Ca_4Co_3O_9$ [52] (2000), and $Bi_2Sr_2Co_2O_9$ [53] (2000) with large Seebeck coefficients, low thermal conductivities (< 1 W/mK) and $ZT \sim 1$ at 700–1000 K. This is a striking contradiction to the common belief that low mobility materials cannot be thermoelectric materials. The most promising candidates for n-type oxide thermoelectric materials include perovskite-type $SrTiO_3$ [54] and $CaMnO_3$ [55]. Yet their *ZT* values are still low, as they have rather high thermal conductivities ($SrTiO_3 \sim 8$ W/mK). By partially substituting Dy for Sr, the thermal conductivity can drop to 3.4 W/mK [56].

2.2 Nanostructured Thermoelectric Materials. Besides the efforts to pursue PGEC in bulk materials, one major direction to improve *ZT* moves towards nanostructuring. Hicks and Dresselhaus [5,6] pioneered the concept that low-dimensional materials can have preferentially modified material properties to enhance *ZT*. The power factor benefits from increased electron density of states near the Fermi level. Thermoelectric materials require dopant optimization to maximize the power factor. For a parabolic electronic band structure, typical for most bulk semiconductors, the slow rise of the density of states near the band edge means that there are only a small number of carriers in this energy range. One must position the Fermi level deeper into the bands to increase the electrical conductivity, yet, as the Fermi level moves deeper into the bands, the Seebeck coefficient decreases because carriers below the Fermi level cancel the entropy carried by carriers above the Fermi level. Hicks and Dresselhaus [5,6] predicted that the sharp density of states in 2D and 1D structures can enhance the power factor. Mahan and Sofo [4] further showed that the ideal electronic density of states to maximize thermoelectric properties was a δ function, although subsequent studies showed that there was an optical bandwidth [57,58]. Mahan and Sofo [4] also identified d- and f-bands as having sharp features in bulk materials. These studies provided strong stimulus for thermoelectric materials research, and many other ideas in electron engineering have been proposed. Resonant

energy levels as represented by Tl-doped PbTe have sharp features in the density-of-states inside the conducting band and have been most successful [59,60]. The energy filtering idea [28], although different from the density-of-states argument, preferentially scatters electrons of lower-energy, which can theoretically lead to higher power factor as well. Experimental evidence for the energy filtering effects was provided in nanogranular PbTe [61] and InGaAs/InGaAlAs superlattices [62]. Other progress was made in improving the electron performance through modulation doping [63], carrier-pocket engineering that produces convergence of different bands in both bulk materials through temperature change [30] and in nanostructures through quantum size effects [64], and antiresonant scattering [65].

The prediction of Hicks and Dresselhaus [5,6] also included strong phonon scattering at interfaces and boundaries to lower thermal conductivity by simply setting the phonon MFPs to be the film thickness. Venkatasubramanian et al. [27] suggested that low-thermal conductivity in the cross-plane direction of superlattices, as experimentally observed [66], can also lead to higher *ZT*. These studies opened a new door for thermoelectric materials research. Although early work focused more on the unique electronic properties stemming from the low dimensionality, it was gradually recognized that a major advantage of nanostructuring is phonon thermal conductivity reduction [67]. This recognition has gone several directions: one is continued studies on individual nanostructures such as nanowires and nanoholes, and another is bulk nanostructures.

Initial experimental focus on low-dimensional structures was on superlattices and quantum wells. Venkatasubramanian et al. [27] reported that p-type Bi_2Te_3/Sb_2Te_3 superlattices exhibit an exceptionally high *ZT* of ~2.4 at room temperature with a remarkably low thermal conductivity of ~0.22 W/mK that is lower than $Bi_{0.5}Sb_{1.5}Te_3$ (~0.5 W/mK). Harman et al. [68] reported quantum-dot superlattices made of PbSeTe/PbTe with a $ZT \sim 2$. We should caution that these data have not been reproduced by other groups. However, it is clear that superlattices have remarkably low thermal conductivity. Si/Ge [69–71], GaAs/AlAs [72], and PbTe/PbSe [73] superlattices were also found and have even lower lattice thermal conductivity than their alloy counterparts.

Parallel to 2D structures, Dresselhaus and coworkers also initiated work on nanowire structures, first demonstrating semimetal to semiconductor transitions as predicted by theory [74]. Later, remarkable lattice thermal conductivity reduction in different nanowires was reported. For example, GaN [75,76], Bi_2Te_3 [77], InSb [78], InAs [79], and Bi [80] nanowires have notable thermal conductivity reduction from phonon-boundary scattering. The most significant claims, however, arise from silicon nanowires. Bulk Si with a high thermal conductivity ~150 W/mK is a poor thermoelectric material with $ZT \sim 0.01$ at room temperature. By dramatically suppressing the lattice thermal conductivity without much disturbance to the power factor, Si nanowires have shown promising *ZT* values. Hochbaum et al. [81] reported $ZT = 0.6$ at room temperature for rough Si nanowires, and Boukai et al. [82] claimed $ZT \sim 1$ at 200 K for Si nanowires, where the thermal conductivities were both reduced to below 2 W/mK.

Other than nanowires made of one pure material, core-shell nanowires [83] or alloyed nanowires [84] may further reduce thermal conductivity. Nanotubes are another 1D nanostructure receiving incremental attention for thermoelectric applications. In fact, nanotubes may reach even lower lattice thermal conductivities than nanowires due to the additional phonon scattering from the holy structure. For example, Bi_2Te_3 nanotubes [85] showed notably low lattice thermal conductivity (~0.3 W/mK) and $ZT \sim 1$.

Guided by the understanding that the reduced thermal conductivity in superlattices was due to diffuse interface scattering rather than phonon band structure modification, Yang and Chen [86] suggested that random 3D nanostructures can be exploited to achieve high *ZT*. At the same time, experiments were emerging with improved *ZT* values in random 3D nanostructures. 3D nanocomposites refer to the format of nanoinclusions such as nanoparticles or nanowires embedded in a host matrix or a heterostructure geometry with nanostructures adjacent to each other. Nanocomposites that do not require any specific morphology are practical for mass fabrication and easy to incorporate into commercial devices. In fact, nanograined materials from the same type usually show desirable thermal conductivity reduction, although these materials often possess additional internal structures such as nanoprecipitates [87]. To preserve the electronic properties, one should also bear in mind that the bandgap between the nanophase and matrix or different nanophases cannot be large.

Two major approaches to make bulk nanocomposites are hot-pressing the ball-milled nanopowers or self-forming inhomogeneities by phase segregation. Ball-milling introduces nanoscale grains within the samples. For example, Lan et al. [9] have reviewed a variety of thermoelectric nanocomposites with promising *ZT* values, including the striking *ZT* of 1.4 for nano-$Bi_xSb_{2-x}Te_3$ [88,89]. Meanwhile, PbTe-based systems have been shown to spontaneously form nanoinclusions within a PbTe rock-salt matrix during thermal processing. For example, in a PbTe-PbS system shape-controlled cubic PbS nanostructures were observed in the PbTe matrix. The considerably low lattice thermal conductivity (~0.7 W/mK at 800 K) was ascribed for a high *ZT* (~1.8 at 800 K) of p-type PbTe-PbS 12% [90]. $NaPb_mSbTe_{2+m}$ (SALT-*m*) is also a high-performance p-type material ($ZT \sim 1.7$ at 650 K). The impressive *ZT* is also attributed to the very low lattice thermal conductivity (0.74 W/mK at 300 K and 0.55 W/mK at 650 K) caused by pervasive nanostructuring [91].

Nanostructured alloys are proven to be powerful in lowering the thermal conductivity by taking advantage of phonon scattering at different length scales. For example, ErAs nanoparticles in an $In_{0.53}Ga_{0.47}As$ matrix [92], nanocrystalline $Bi_xSb_{2-x}Te_3$ [88,89] and $Si_{0.8}Ge_{0.2}$ [32], and nanostructured $Bi_{2-x}Cu_xS_3$ [93] have been demonstrated to possess the thermal conductivity 30–50% lower than the alloy limit. The same idea can also be extended to nanostructured phonon rattling materials. For example, nanostructured $Yb_{0.3}Co_4Sb_{12+y}$ was reported to have a $ZT \sim 1.3$ at 800 K [94]. InSb nanophase with grain sizes ranging from 10–80 nm in $In_xCe_yCo_4Sb_{12}$ lead to a notable depression of lattice thermal conductivity and a $ZT \sim 1.43$ at 800 K [95].

Figure 1 summarizes *ZT* values for different materials (plots both n-type and p-type).[1] Considering that the highest *ZT* values before the 1990s were around 1, progress in thermoelectric materials is indeed very impressive. Many improvements come from reduced lattice thermal conductivity, which will be discussed in the next few sections. In the following sections, we will first

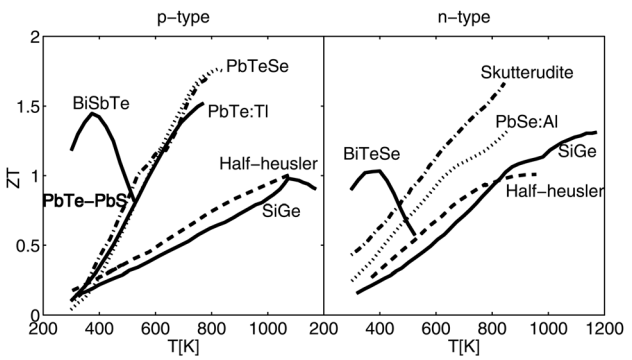

Fig. 1 Figure of merit *ZT* of selected state of the art thermoelectric materials versus temperature for (*a*) p-type and (*b*) n-type. (p-type: $Si_{0.8}Ge_{0.2}$ [33], $Bi_{0.5}Sb_{1.5}Te_3$ [88], 2% Tl-doped PbTe [59], Na-doped $PbTe_{0.85}Se_{0.15}$ [30], Na-doped PbTe-PbS 12% [90], half-Heusler $Hf_{0.8}Ti_{0.2}CoSb_{0.8}Sn_{0.2}$ [50]; n-type: $Si_{0.8}Ge_{0.2}$ [32], multifilled skutterudites $Ba_xLa_yYb_zCo_4Sb_{12}$ [39], half-Heusler $Hf_{0.75}Ti_{0.25}NiSn_{0.99}Sb_{0.01}$ [49], 1% Al-doped PbSe [60], $Bi_2Te_{2.7}Se_{0.3}$ [96].)

[1]References cited in Figure 1 are [30,32,33,39,49,50,59,60,88,90,96].

discuss heat conduction mechanisms in bulk crystals (Sec. 3) and then move on to discuss strategies and corresponding mechanisms used in reducing thermal conductivity in both bulk materials (Sec. 4) and nanostructures (Sec. 5).

3 Heat Conduction in Bulk Thermoelectric Materials

In typical semiconductors, the electronic contribution to thermal conductivity is usually masked by the phononic contribution, although the electronic contribution to thermal conductivity also becomes appreciable in materials with high ZT values. In this section, we will discuss heat conduction mechanisms in bulk crystals.

3.1 Heat Conduction by Phonons. Understanding heat conduction in crystalline solids started only when the quantum theory of lattice vibration was developed and the phonon concept was established. The basic quantum of crystal lattice vibration is called a phonon. The phonon scattering originating from the anharmonic interatomic potential can be classified as either a normal process, which conserves crystal momentum, or an umklapp process, which does not. It was recognized that the umklapp process creates a resistance to heat flow while the normal process only redistributes phonons. Peierls [97] extended the Boltzmann formulation for phonon transport taking into consideration only the umklapp process. Under the relaxation time approximation and assuming isotropic group velocity and phonon lifetime, the Boltzmann equation led to the kinetic theory expression for thermal conductivity as

$$\kappa_p = \frac{1}{3}\int_0^{\omega_{\max}} C(\omega)v(\omega)\Lambda(\omega)d\omega = \frac{1}{3}\int_0^{\omega_{\max}} C(\omega)v^2(\omega)\tau(\omega)d\omega \tag{2}$$

where $C(\omega) = \hbar\omega D(\omega)df_{BE}/dT$ is the specific heat per unit frequency interval at frequency ω and temperature T, $D(\omega)$ is phonon density of states per unit volume and per unit frequency interval, f_{BE} is the Bose–Einstein distribution, v is the phonon group velocity, $\Lambda = v\tau$ is the phonon mean free path (MFP), and τ is the phonon lifetime. Callaway [98] further modified the theory by accounting for both the normal and umklapp scattering processes, assuming that normal processes lead to a displaced Bose–Einstein distribution and indirectly affect the umklapp processes. The derived expression is similar to Eq. (2) except for a modification to phonon lifetimes. The quantities in Eq. (2) that determine the lattice thermal conductivity, however, are frequency dependent and difficult to obtain. Different approximations were made to perform the thermal conductivity integral.

First, the Debye approximation that assumes a linear relation between the phonon frequency and the propagation wavevector is often used for the phonon group velocity and density of states, based on the fact that the Debye approximation has been very successfully used to explain the specific heat of crystalline materials. This left the phonon lifetime unknown. In the 1950s, Klemens [99] derived expressions using the quantum perturbation theory, i.e., Fermi's golden rule, for phonon lifetimes due to different scattering mechanisms. The expressions obtained are again based on the Debye approximation and contains unknown parameters. The experimental values of thermal conductivity, speed of sound, and specific heat are often used to fit the unknown parameters in the Debye model and in the lifetimes. Such fittings usually work well at low temperatures. Deviations at high temperatures stimulated more refined models of dispersion, such as the one developed by Holland [100] that used two different linear dispersions to better represent the rapid flattening of transverse acoustic phonons in FCC crystals such as GaAs and Si.

The shape of the temperature dependence of thermal conductivity is universal among crystalline solids. At high temperatures, thermal conductivity usually decreases with increasing temperature as T^{-n}, with theoretically $n=1$ although practically $n=1$–1.5. This is because at high temperatures, phonon specific heat is a constant according to the Pettit–Delong law, and phonon energy, i.e., the number of phonons, increases linearly with temperature. As the scattering rate is proportional to the number of phonons, the thermal conductivity decreases with increasing temperature. At low temperatures, the thermal conductivity is usually proportional to T^3. In this regime, phonon-phonon scattering is weak and phonon MFPs are longer than the size of the sample. Phonons scatter more frequently with the boundaries, and the phonon MFP is effectively equal to the sample size and is independent of frequency. Thermal conductivity is thus proportional to the specific heat and hence the T^3 behavior. This size effect was first discovered by de Haas and Biermasz [101] and explained by Casimir [102] (sometimes called the Casimir regime). Casimir assumed that surfaces of samples are rough and scatter phonons diffusely, although latter studies also investigated partially diffuse and partially specular surfaces [103]. In between low and high temperatures, impurity scattering is usually important, and the peak value of thermal conductivity depends sensitively on impurity concentrations.

Although the approaches pioneered by Klemens were successful in explaining the trend of experimental observations, quantitative details of phonon transport may be far from what the past approaches described above predicted, especially in terms of the phonon lifetimes and MFPs. The reason that the Debye model together with Klemens' treatment on scattering can fit experimental data is because the thermal conductivity integral is quite forgiving. In fact, one can use different sets of parameters to fit the experimental data based on different approximations. Extracting the exact phonon transport properties, especially phonon lifetimes and MFPs, was thus unsolved.

Since the 1980s, efforts started on calculating thermal conductivity of crystals using molecular dynamics (MD) simulations [104–108]. In classical MD, the approximate trajectories of each individual atom within the simulation domain are tracked based on an empirical interatomic potential and Newton's second law. Two prevailing methods used to study heat transport are equilibrium molecular dynamics (EMD) and nonequilibrium molecular dynamics (NEMD). EMD is suitable for transport properties, whereas NEMD simulates actual transport processes. EMD first obtains the history of individual particles in an equilibrium system, from which the transport properties are extracted on the basis of linear response theory. The thermal conductivity is calculated from the autocorrelation of the instantaneous heat flux through the Green–Kubo formula [109,110]. For NEMD, one can either impose a temperature difference to calculate the heat flux [111] or impose a heat flux to calculate the resulting temperature distribution [112,113]. The thermal conductivity is then determined by the Fourier's law. The NEMD methods are relatively easy to implement and are usually faster than the EMD methods because the latter requires the calculation of the autocorrelation function, which can take a long time to decay. In addition, the EMD method may involve the artificial autocorrelation caused by often-used periodic boundary condition. However, NEMD also suffers from several drawbacks. Firstly, the statistical foundation of NEMD is not as soundly established as that of EMD [114]. Second, the finite simulation size in NEMD might be shorter than the MFP of some phonon modes, leading to artificial size effects with boundaries imposed at the heat reservoirs. Third, a large temperature difference is applied across a small simulation domain.

To extract the phonon lifetimes and MFPs, the phonon spectral energy density analysis [115–118] has been applied in combination with EMD. The key idea is to project the atomic displacements onto normal mode coordinates and determine the phonon lifetimes by tracing the temporal amplitude decay of each mode or fitting the width of spectral energy density peaks in the frequency domain. To apply this approach, one needs to utilize eigenvalues and eigenvectors from lattice dynamics calculations and perform a separate analysis from the traditional thermal conductivity calculations using MD.

As a widely adopted simulation tool, MD simulations do not require any a priori knowledge of the phonon transport properties,

are straightforward to implement, and automatically include the temperature-dependent anharmonicity. Yet MD is only rigorously applicable to solids above the Debye temperature for being entirely classical that assumes each vibration mode is equally excited. At low temperatures, quantum correction to temperature is needed. The electronic contribution to thermal transport cannot be assessed in MD. Moreover, the empirical potentials used in classical MD can cause the thermal conductivity to deviate significantly from the experimental data [119].

Conversely, first-principles calculations where the potential is obtained directly from the electron charge density via density functional theory (DFT) without any adjustable parameters provide a most reliable way of computing the lattice thermal conductivity. Ab initio MD simulations [120,121] use the forces computed on-the-fly by DFT and are computationally expensive, though. The alternative way is to extract the interatomic force constants from DFT calculations of limited atomic configurations and conduct further calculations. After DFT calculations, one can either obtain the force constants from reciprocal space based on the density functional perturbation theory (DFPT) [122,123] or from real space by fitting the force-displacement data in a supercell with a polynomial potential [124,125]. Despite the fact that the real space approach is simpler yet less precise, both approaches are accurate enough to reproduce the experimental results of lattice thermal conductivity as shown in Fig. 2(*a*). Broido et al. [122] calculated the intrinsic lattice thermal conductivity of Si and Ge using reciprocal space approach and obtained excellent agreements with experimental data. The reciprocal approach was later applied to Si_xGe_{1-x} alloys and superlattices by Garg et al. [126,127], and PbSe, PbTe, and $PbTe_{1-x}Se_x$ by Tian et al. [128]. Esfarjani et al. [125] started the real space approach with Si and then extended to half-Heusler [129], PbTe [130], and GaAs [131].

Once the harmonic and anharmonic force constants are obtained, one can either perform MD simulations based on developed Taylor expansion potential [129] or employ lattice dynamics calculations: first obtain the vibrational eigenmodes based on the harmonic part of the potential, then compute the scattering rates of each mode by treating the anharmonic potential as a perturbation using Fermi's golden rule and solving the Boltzmann transport equation (BTE) to find the thermal conductivity [122,125–130]. Although MD simulations based on fitted potentials have more flexibility to directly obtain the lattice thermal conductivity on complicated structures, lattice dynamics calculations can produce the detailed phonon transport properties without extra efforts because the thermal conductivities are the integrated quantities over the first Brillouin zone using either the solution of BTE under single-mode relaxation time approximation [125,126,128–130,132] or based on an iterative solution of the integral BTE [122].

Fundamental phonon transport properties are crucial for further reducing the thermal conductivity and enhancing *ZT*. The thermal conductivity accumulation as a function of phonon MFPs from first-principles calculations is shown in Fig. 2(*b*).[2] The phonon MFPs in a material span a wide range of magnitudes, from nanometers to microns. Different materials possess different MFP distributions that can provide insight on the required length-scale of nanostructuring to effectively lower the thermal conductivity. For example, while nanostructures of 100 nm can efficiently reduce the thermal conductivity of Si and GaAs, nanostructures of less than 10 nm are needed for PbTe and PbSe.

Experimental determination of detailed phonon transport properties is more challenging. Encouraging progress is emerging, though. Using Raman spectroscopy [134,135], inelastic neutron scattering [136], or inelastic X-ray scattering [137], the phonon lifetimes can be extracted from peak width. However, Raman process can only probe certain first-order zone center or second-order zone edge modes, while the other two measurements only work on bulk single crystals as one needs to distinguish each incident

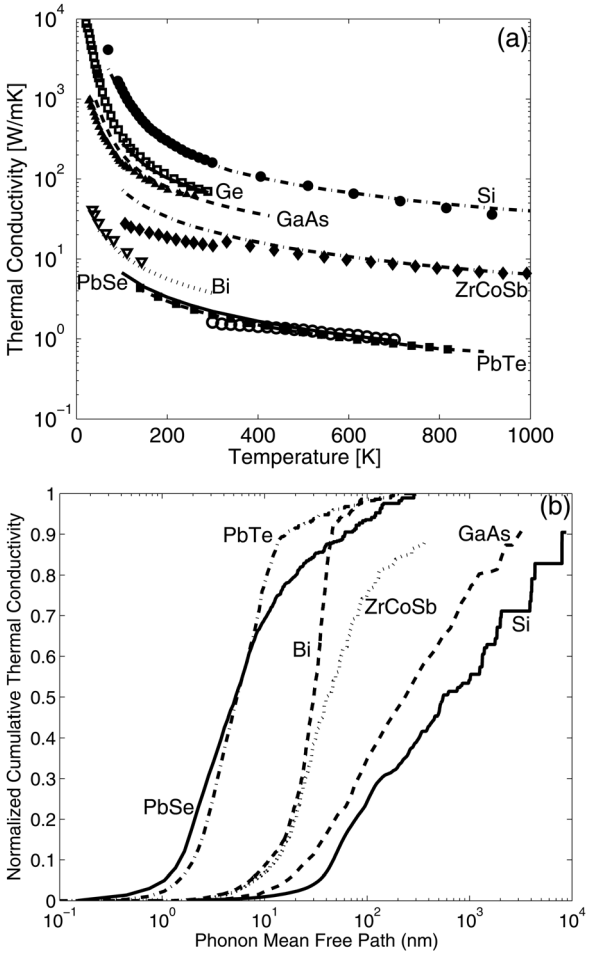

Fig. 2 (*a*) Thermal conductivity versus temperature from first-principles calculations (lines) and experimental measurements (symbols), and (*b*) normalized cumulative thermal conductivity as a function of phonon MFPs at 300 K from first-principles calculations for different bulk crystalline materials, Si [125], Ge [122], GaAs [131], ZrCoSb [129], PbTe [128], PbSe [128], and Bi [133]

wavevector of neutrons or X-rays. Recent developments in different laboratories have opened new ways to directly determine the thermal conductivity integral in the form of integration over MFPs [115,138]. In time-domain thermoreflectance (TDTR) measurements, Koh and Cahill [139] observed modulation frequency dependence in alloy-based samples. They assumed that phonons with MFPs longer than the thermal penetration traverse ballistically and do not contribute to the measured thermal conductivity, which is fitted to a diffusive model. BTE simulation, nevertheless, cannot explain their experimental results [140]. Minnich et al. [132] mapped out the accumulative thermal conductivity with respect to phonon MFPs using TDTR by varying the pump beam sizes. The key idea is that the heat flux from a heat source will be smaller than Fourier's law's prediction if some phonon MFPs are longer than the heater size such that their transport is ballistic [141]. This was confirmed experimentally using a soft X-ray transient grating method to probe heat flow from nanolines to a substrate [142]. Transient thermal grating experiments can also excite the quasi-ballistic regime by controlling the grating spacing, and the MFP information can be inferred [143]. By numerically inverting the integral function of the total thermal conductivity, Minnich [144] managed to reconstruct the thermal conductivity accumulation curve as a function of MFPs from the measured data without any assumptions about the phonon scattering mechanism. Efforts to push characteristic experimental lengths down to the nanoscale in order to collect the whole range

[2]References cited in Figure 2 are [122,125,128,129,131,133].

of MFPs and observe the size dependence at elevated temperatures would bring the experimental demonstration to a more complete level.

Detailed phonon transport properties studied both theoretically and experimentally not only provide insights on the effectiveness of nanostructuring to reduce thermal conductivity as discussed above but also deepen our understanding of transport processes. For example, lead chalcogenides have a high-symmetry rock-salt structure yet surprisingly low thermal conductivity ($\sim$2 W/mK) at room temperature. This has intrigued studies on the origin of low thermal conductivity in PbTe and PbSe [128,130,136]. From both first-principle calculations and inelastic neutron scattering experiments, it was found that the strong coupling between acoustic and optical phonon modes and the soft TA modes, in addition to the heavy mass, were the reasons for low thermal conductivity. The phonon transport physics in pure bulk materials thus serves as the fundamental platform for us to further explore the heat conduction in the more complicated structures.

3.2 Heat Conduction by Electrons. In addition to phonons, electrons also carry heat in thermoelectric materials as implied by the Peltier effect. As all the electronic transport coefficients are related to the scattering rate, the electronic thermal conductivity can be related to the electrical conductivity through the Wiedemann–Franz law ($\kappa_e = L\sigma T$). Most good thermoelectric materials are heavily doped semiconductors to achieve high electrical conductivity. Hence, heat conduction by electrons cannot be neglected in thermoelectric materials and becomes even more significant near the temperature where ZT peaks.

The electronic contribution to thermal conductivity contains two parts. One is due to each individual electrons/holes as determined by the Wiedemann–Franz law. The other is due to energy difference across the bands, called the bipolar contribution. As electrons and holes diffuse from high temperature to low temperature regions, carrier concentration must change and recombination happens, releasing energy across the bandgap. The total electronic thermal conductivity can be expressed as [24]

$$\kappa_e = \kappa_n + \kappa_p + \frac{\sigma_n \sigma_p}{\sigma_n + \sigma_p}(S_n - S_p)^2 T \tag{3}$$

In the expression above, the third term shows the bipolar heat conduction. In nondegenerate limit and under constant relaxation time approximation, we can easily show that $S_n - S_p$ is proportional to the bandgap energy. The bipolar contribution to thermal conductivity is significant at high temperatures when the semiconductor becomes intrinsic such that both σ_n and σ_p are large. Typically, one observes measured thermal conductivity of a good thermoelectric material first decreases with increasing temperature, due to the decreasing trends of phononic contribution, and then increases with increasing temperature, a sign of the onset of bipolar contribution. This trend applies for most of the temperature range except for very low temperatures where phonon scattering by impurities or boundaries is dominant. The electronic contribution to total thermal conductivity is usually small compared to lattice contribution (less than 10%), but the bipolar contribution can be significant and even comparable to the lattice contribution at higher temperatures where semiconductor becomes intrinsic.

Reducing electronic and bipolar thermal conductivity would improve ZT, but it remains a challenging problem due to strongly coupled transport characteristics. One possible way, having not been demonstrated experimentally, is to modify the density-of-states near the Fermi level to make a δ function shape [4,145]. The maximal ZT condition corresponds to the limit when the Lorenz number is zero. To reduce the bipolar effect, one possible way is to preferentially deteriorate minor carrier's electrical conductivity or Seebeck coefficient.

Even though the electronic heat conduction is considerable in thermoelectric materials, it is not easy to quantify the electronic contribution to total heat conduction. The most widely used method is the Wiedemann–Franz law. However, the Lorenz number ($L = 2.45 \times 10^{-8} \mathrm{W\Omega/K^2}$) in the Wiedemann–Franz law is based on metallic electron transport. In semiconductors, the Lorenz number depends on carrier density and electron scattering [146]. More importantly, the Wiedemann–Franz law cannot describe the bipolar thermal diffusion correctly since the bandgap is not included in its derivation. Instead of the using the Wiedemann–Franz law with the Lorenz number for metals, one can measure several electronic transport properties, deduce electronic transport parameters, and then calculate the electronic thermal conductivity [147,148]. Single band approximation is often used to reduce the number of fitting parameters, but it is not applicable for near ZT peak temperature and materials having multiple valleys such as $PbTe_{1-x}Se_x$ [30]. Another more direct way is to measure thermal conductivity under low temperatures and high magnetic fields. In this case, the electronic heat conduction is highly suppressed and the measured thermal conductivity mostly comes from phonon contribution [149]. However, this method is limited only for low temperatures and requires large facility for high magnetic fields. In addition, if a material has large thermomagnetic effects like Bi and Bi_2Te_3, then a careful correction for thermomagnetic effects should be also included [150]. Therefore, characterizing electronic heat conduction is not straightforward, and a better method should be developed to understand and control electronic heat conduction.

4 Thermal Conductivity Reduction in Bulk Materials

To reduce the lattice thermal conductivity in bulk thermoelectric materials, two major strategies, alloying [26] and introducing phonon rattlers [1], were proposed in the 1950s and the 1990s, respectively. Although their appearances were 40 years apart, both alloy and phonon rattler essentially share the same idea: introducing atomic disorder either substitutionally or interstitially. In this session, we will focus on the fundamental mechanism, the current understanding, and the remaining questions of the two approaches.

4.1 Alloy. Alloying is the traditional and probably the easiest way to reduce the lattice thermal conductivity without much degradation to the electrical conductivity. By substituting lattice sites with different atoms, especially atoms in the same column of the periodic table with similar electronic structures, the impurities can more strongly scatter short wavelength phonons than electrons, resulting in greatly reduced lattice thermal conductivity and well-preserved electronic properties. The alloying effect is particularly large when the mass ratio between the matrix atom and substitutional atom is large. For example, the lattice thermal conductivities of Si and Ge at 300 K are rather high ($\sim$150 W/mK and $\sim$60 W/mK). The measured thermal conductivity of $Si_{1-x}Ge_x$ can sharply fall down to below $\sim$10 W/mK [25], which led $Si_{1-x}Ge_x$ to become a useful thermoelectric material.

Theoretical studies of phonon transport in alloy systems are limited due to the breakage of the long-range translational symmetry. Thermal conductivities of alloys are typically modeled using the virtual crystal approach introduced by Abeles [151], assuming that the alloy forms a new crystal that is an average of the crystal structures of the constituent materials and has its own corresponding dispersion. The mass disorder and anharmonicity are both treated as first-order perturbations. Thermal conductivity is modeled following the approaches of Callaway [98] and Klemens [99], using Matthiessen's rule to combine different scattering mechanisms. Reduction in thermal conductivity is included in the scattering mechanism. The phonon impurity scattering rate is usually taken into account using the Rayleigh scattering model [152] in which the scattering rate is assumed to be proportional to the fourth power of the phonon frequency with the proportionality constant depending on the mass difference and the atomic volume contrast, or using the improved Tamura model that incorporates

the actual phonon density of states [153]. Using force constants from DFPT in combination with the virtual crystal model, Garg et al. [126] were able to well reproduce the experimental thermal conductivity of $Si_{1-x}Ge_x$. The same approach has also been applied to $PbTe_{1-x}Se_x$ [128]. Using force constants from first-principles calculations while varying the atomic masses to account for different half-Heusler alloys, Yan et al. [50] and Shiomi et al. [129] performed EMD simulations and reached reasonably good agreement with experiments.

Despite the success of the virtual crystal model in matching experimental data, questions regarding its validity remain. First, Rayleigh scattering is only applicable when the wavelength is much longer than the defect dimension [154], which is on the order of atomic sizes for alloys. For high frequency phonons the Rayleigh model may not be valid. Second, in the Abeles model [151], atomic mass difference relative to the virtual crystal does not distinguish whether the impurities are heavier or lighter, which does not take into account whether the scatterer frequency is within or above the phonon bands of the matrix. Moreover, it is unclear how the scattering picture transitions from isolated scatterers in the dilute limit to dependent scattering in the nondilute mixing limit, which is similar to localized and extended states in electronic materials [155,156]. Additionally, the proper treatment of phonon group velocities is under debate. Therefore, a thorough understanding of alloy systems is needed.

4.2 Phonon Rattler. Slack [3] proposed that skutterudites with open cages can be filled with other atoms, which oscillate locally to scatter phonons in the host. Unlike the guest atoms in alloys, which form normal crystal bonds, the guest atoms serving as phonon rattlers are weakly bonded to the oversized cage structure and vibrate locally. Although the rattling idea has led to large progress in *ZT* of skutterudites, understanding how these extrinsic atoms reduce thermal conductivity has been debated and is still not fully clear.

First, within the phonon rattling picture, there have been different views on whether the localized modes of guest atoms acting alone or the resonant phonon scattering essentially causes the low thermal conductivity. Sales et al. [157] suggested that the localized incoherent vibration of guest atoms were responsible for the large reduction in thermal conductivity. The rattler induced localized modes were experimentally observed in filled skutterudites by inelastic neutron scattering [158] and nuclear inelastic scattering [159]. On the other hand, a resonant scattering picture was proposed [160], in which only those phonons with frequencies close to the localized rattler frequency would strongly interact with the local mode. Inelastic neutron scattering experiments suggested that fillers of different chemical nature in multifilled skutterudites provided a broader range of resonant scattering as the quasi-localized modes of fillers were at frequencies sufficiently different from one another [161]. Wang et al. [162] conducted ultrafast time-resolved optical measurements to investigate vibrational behaviors of filled antimony skutterudites in time domain. They identified resonant interaction between guest and host atoms as the main cause for the thermal conductivity reduction.

Second, there are additional factors including lattice disorder and point defects, which cannot be decoupled from the rattling effect. Although Slack's idea is that the filler atoms jiggle in the cage at a distinct frequency to scatter phonons of the host, Meisner et al. [163] proposed that the reduced thermal conductivity can also be explained by the virtual crystal model. The even stronger reduction in the thermal conductivity of multifilled skutterudites may also be attributed to the additional point defect scattering from the extra mass fluctuation at the void site [164].

Third, the disordered glass-like picture by rattling modes was questioned by the quasi-harmonic behavior observed by Koza et al. [165]. They found coherent coupling between the filler atoms and the host lattice in $LaFe_4Sb_{12}$ and $CeFeb_4Sb_{12}$ using neutron scattering experiments and ab initio powder-averaged lattice dynamics calculations. Their finding defied the rattling picture of filler atoms. The coherent low energy phonon modes were thus believed to preserve the phonon crystallinity and contribute to the relatively high thermal conductivity in p-type skutterudites. Zebarjadi et al. [166] applied MD simulations for the thermal conductivity of filled skutterudites with a simple 2D model. It was found that the decay of the thermal conductivity mainly comes from the flattening of phonon bands, i.e., smaller phonon group velocity, due to the filler atoms.

These controversies, together with the puzzling alloy picture discussed earlier, means that we do not fully understand how impurities in crystals go from individual isolated scattering centers to forming new band structures.

5 Thermal Conductivity Reduction in Nanostructured Materials

In this section, we will explore the thermal conductivity reduction in different nanostructures with the goal of harnessing phonon scattering while leaving electronic properties unaffected. Unlike alloys, which scatter very short wavelength phonons, nanostructures can scatter longer wavelength phonons over a wider range at interfaces and surfaces and effectively suppress the thermal conductivity.

5.1 1D Nanostructure: Nanowires. Li et al. [167] conducted the first thermal conductivity measurement of individual Si nanowires and observed 2 orders of magnitude reduction from the bulk value. Subsequent experiments on rough Si nanowires [81] reported even lower thermal conductivity, close to the amorphous limit. Other types of nanowires have also been reported to have lower thermal conductivities [75–80]. Phonon-boundary scattering can readily account for the thermal conductivity reduction in most nanowires reported in literature. Several theoretical calculations using MD [168–171], BTE solution [172–178], and Landauer formalism [179,180] have been carried out and reached good agreements with experimental data for smooth Si nanowire with diameters >20 nm. Nevertheless, the physical picture underlying the lower than expected experimental thermal conductivity and the surprising linear temperature dependence of Si nanowires [167] and Ge nanowires [83] with diameters $\sim$20 nm and the phonon-roughness scattering effects [81] are thus far not fully explored. Admittedly, the measurements of thin nanowires are very sensitive to nonuniformity of the sample diameters and to surface conditions, which become more difficult to control as diameters decrease. This uncertainty adds to the complexity for theoretical modeling even though the surface roughness effects have recently been quantified experimentally for Si nanowires with diameters $\sim$70 nm [181].

The theoretical difficulties mainly lie in the proper treatment of phonon-boundary scattering and phonon confinement effects. Although MD simulations automatically incorporate both phonon confinement and boundary scattering effects, the diameter that can be simulated is limited. How the surface roughness affects the phonon confinement, in addition to specular or diffuse interface scattering, are open questions. One key challenge is how one can build proper surface structures to best represent the experimental samples. Besides, the accurate modeling of intrinsic phonon lifetimes from first-principles calculations [125,173], the importance of optical phonons in nanowires [173], the core defects, and the surface oxide layer [170] should also be considered.

5.2 2D Nanostructure: Thin-Film Superlattices. Quantum well and superlattices were studied to enhance the Seebeck coefficient via the sharp feature in the electron density of states and to reduce the lattice thermal conductivity. Surprisingly, the thermal conductivity of superlattices was able to be reduced to below the alloy limit [69–73]. Chen [67] argued that the minimum thermal conductivity theory proposed by Slack [182] and Cahill et al.

[183] may not apply to low-dimensional materials due to the directionally dependent phonon properties arising from the anisotropy, such as, angularly dependent reflectance at interfaces and provided some initial evidence based on Si/Ge superlattices. Conclusive data was provided by Cahill's group [184,185].

In addition to superlattices, thermal conductivity of individual thin films has also been studied, especially Si films. Goodson and his coworkers [186–189] systematically measured the thermal conductivity of Si thin films down to 74 nm. Their modeling showed that the Fuchs–Sonderheim model on classical size effects can well explain the experimental data, which is quite different from the controversies in Si nanowires. More recently, ultrathin Si films down to 8 nm were used to extract phonon dispersions [190] and phonon lifetimes [191] and to observe quasi-ballistic transport [192].

Theories developed to understand the large thermal conductivity reduction in superlattices can be categorized into an incoherent particle picture and a coherent wave picture. By solving the BTE for partially specular and partially diffuse interface scattering of phonons under the relaxation time approximation, Chen [193,194] concluded that the diffuse and inelastic interface scattering was responsible for the strong thermal conductivity reduction of Si/Ge [69] and GaAs/AlAs [72] superlattices. Another picture is coherent transport. The new periodicity in the superlattice introduces modified phonon dispersions, including miniband formation originating from interference of phonon waves [195], phonon confinement arising from spectra mismatch [196], and group velocity reduction due to phonon reflection [197]. These effects lead to decreased thermal conductivity in the direction perpendicular to the film plane [198] but do not significantly reduce the in-plane thermal conductivity. As period size approaches the extremely small periods, phonon tunneling or simply alloying [198] leads to a recovery of thermal conductivity with decreasing period thickness. Models based on perfect interfaces and phonon dispersion modification, however, generally cannot explain the experimental data observed in both in-plane and cross-plane directions [199], suggesting the importance of interface roughness. Combining the wave and particle pictures using models [200,201] or MD simulation [202], one can explain the observed trends in different superlattices [69,71–73] that the thermal conductivity decreases first as period size increases, reaches a minimum at a few nanometers, and then increases with increasing period size.

Although diffuse scattering at interfaces was responsible for thermal conductivity reduction, past BTE based models still assume a specular component [193], i.e., partially specular and partially diffuse interfaces. A key question is whether one can observe coherent phonon contributions to thermal conductivity. In general, wave effects on thermal conductivity have not been demonstrated clearly [193], although their importance was speculated in some past experiments in nanowires [167] and nanomesh structures [203]. To answer this question, Luckyanova et al. [204] measured thermal conductivities of superlattices by fixing the period length while changing the number of periods. If the interface scattering is completely diffuse, they expect to see a thermal conductivity independent of the number of periods. If transport is coherent, they expected to see that thermal conductivity increases linearly with the total thickness of the superlattice. The observed length dependence of thermal conductivity, together with lattice dynamics based simulation, shows that low-frequency phonons actually have much longer MFPs than the total thickness of superlattice, and their transport is coherent. If one can destroy the coherence of these low frequency phonons, further reduction in the lattice thermal conductivity is possible.

5.3 3D/Bulk Nanostructures: Nanocomposites. Based on the superlattice studies, periodicity is not essential for the thermal conductivity reduction whereas interface scattering creates a more profound decrease [67]. Nanocomposites with a high density of interfaces offer a cost-effective alternative to superlattices as potential thermoelectric materials. Simulation further suggests that the thermal conductivity of nanocomposites can reach below the alloy limit [205]. The presence of nanoparticles provides an effective scattering mechanism for mid/long wavelength phonons that contribute heavily to the thermal conductivity.

The theoretical studies on phonon transport in nanocomposites are rather demanding. Kim and Majumdar [206] proposed an approximate analytical solution to estimate the phonon scattering cross section of very small nanoparticles ($d = 4$ nm) by bridging the Rayleigh limit and the geometrical scattering limit. They found that large size distribution can more efficiently scatter phonons of a wide range of spectra. Monte Carlo simulation by McGaughey and Jain [207] on polycrystalline bulk Si with grain sizes around 0.1–1 μm shows that a larger size distribution leads to larger thermal conductivity assuming diffuse boundary scattering for each grain.

To treat thermal transport in nanocomposites, the first thing one needs to address is phonon transport across interfaces as phonon reflections at the interfaces create interfacial resistance. Thermal boundary resistance depends on the phonon equilibrium density and the phonon transmittance across the interface. The unknown interface condition of the experimental samples adds major complexity for understanding and predicting interfacial transport. Phonon interface transmittance models have yet to reliably predict experimental observations. There are two different models for the phonon transmittance at an interface: the acoustic mismatch model (AMM) [208] and the diffuse mismatch model (DMM) [209]. As a continuum model, the AMM assumes that phonons undergo specular reflection or transmission at the interface and is valid in the long-wavelength limit. The DMM, on the other hand, assumes not only purely diffuse scattering at the interface but also equivalence between phonon reflectance from one side to the transmittance from the other. Both AMM and DMM have several assumptions that lose their validity rapidly as the temperature and material complexity increases. Using MD at zero temperature [210–213], wave-packets can be created and the phonon transmittance can be obtained by tracking the energy transmitted and reflected after encountering an interface. Although easy to implement, it is computationally expensive and cannot capture a wide angle of incidence, which requires a large lateral size that is difficult to achieve in MD simulations. Linear lattice dynamics calculations [214–217] have been performed to extract the mode-dependent phonon transmittance by solving the reflected and transmitted wave functions according to boundary conditions. However, this method is difficult to implement for complex atomic structures. As an alternative and more computationally efficient approach, a Green's function method dedicated to solve for the response from a point source perturbation is employed to compute the phonon transmission function that can be easily related to transmittance via dividing the transmission function across an interface by its counterpart in the incident material. A general formulation and full derivation have been detailed by Zhang et al., and Volz [218–220], and applied to different materials [221–226]. Tian et al. [225] applied the first-principles based Green's function approach to investigate single interfaces between bulk 3D Si and Ge and found that the effects of interface roughness stemming from atomic mixing can even enhance the phonon transmittance due to a smoother transition of the density of states. This conclusion does not conflict with the discussion in Sec. 5.2 that diffuse scattering reduces thermal conductivity of superlattices since diffuse scattering destroys the coherence of phonons in superlattices.

The theoretical efforts to access the effective thermal conductivity of nanocomposites mainly fall into three categories: the effective medium approach (EMA), molecular dynamics simulations, and the Boltzmann transport equation. Nan et al. [227] developed a general effective medium approach for the effective thermal conductivity of arbitrary particulate composites. However, this macroscopic model is based on diffusive transport theory that is not always valid at the nanoscale. Minnich and Chen [228] derived a modified EMA formulation for spherical

particulate nanocomposites by including the interface density. Their results showed that the interface density dominated the effective thermal conductivity in nanocomposites, where the thermal boundary resistance played a critical role. Ordonez-Miranda et al. [229] extended the modified EMA model of Minnich and Chen [228] for spheroidal inclusions. EMA is convenient to employ, but it requires thermal boundary resistance as an input and it becomes difficult to deal with complicated nanostructures.

Molecular dynamics simulations, on the other hand, allow the direct calculation of thermal boundary resistance across different interfaces [230–233] and the effective thermal conductivity of various nanocomposites [233–235]. Nevertheless, the thermal boundary resistance determined from MD is an integral quantity, which cannot provide the detailed phonon behaviors at interfaces. The empirical potentials adopted in MD simulations also hold it back to a certain extent. The small accessible size of the MD method continues to be the main obstacle of their usefulness in complicated composite nanostructures.

Yang and Chen [86] computed the effective thermal conductivity of a periodic two-dimensional nanocomposite with square silicon nanowires in germanium by numerically solving the BTE under a single mode relaxation time approximation. It was demonstrated that for a fixed silicon wire dimension, the lower the atomic percentage of germanium, the lower the effective thermal conductivity of the nanocomposites, opposite to the macroscale observation. Prasher [236] solved the BTE analytically for simple geometries. For more complicated nanostructures, Monte Carlo (MC) simulation is a useful tool to solve the BTE by tracking the phonon energy bundles as they drift and collide through the computational domain. Jeng et al. [237] used MC simulations to study 3D phonon transport in nanocomposites using a gray-medium approach and showed that the effective thermal conductivity of nanocomposites can reach below the alloy limit [92]. More efficient MC techniques using energy-based variance-reduction were developed to simulate multidimensional phonon transport [238,239].

The BTE and MC examples described above assume frequency independent MFP and diffuse interface scattering. To accurately model the phonon transport in complex nanostructured materials, the mode-dependent phonon MFPs and interface transmittance from first-principles calculations are desired. Simulation tools already developed, such as extracting the MFPs from first-principles and phonon transmittance from the Green's function method, can in theory provide these input parameters. However, a key challenge is to relate interface conditions to simulations. Past experiments [240] and modeling [241] show that the thermal boundary resistance depends sensitively on imperfections. With the excellent advances on bulk phonon MFPs and encouraging progress on interface transmittance, both from DFT, multiscale simulation of phonon transport in nanostructures is in sight.

6 Heat Transfer in Thermoelectric Devices and Systems

Even if thermoelectric materials with high *ZT* are developed, there are still many device-level challenges to implement thermoelectrics into real applications. In fabricating thermoelectric modules, many technical issues like durability and parasitic losses should be considered. In designing whole systems, heat transfer control should be included to match the heat flux between the heat sink/source and thermoelectric modules. In fact, for many applications, one should consider the device together with the system because system requirements may affect device design. Innovative applications of current materials, although not competitive in prime power and HVAC, are crucial for thermoelectric technology and arguably even more urgent than improving *ZT*. In this section, we discuss heat transfer related issues in thermoelectric modules and systems.

6.1 Thermoelectric Devices. In the actual thermoelectric module, there are many layers such as a diffusion barrier between an interconnector and a thermoelectric pellet. These additional layers introduce electrical and thermal resistances due to their finite thickness and also due to the mismatch of electronic properties at the interfaces, which can significantly reduce the efficiency below that of ideal device expressions. Due to such resistances, thermoelectric devices should not be made very thin [24]. Min and Rowe [242] further considered thermal/electrical contact resistances in the coefficient of performance (COP) calculation of thin film thermoelectrics and showed total efficiency can be largely deteriorated by contact resistances. A recent report on direct on-chip cooling by thermoelectrics shows thermal contact resistance is more important than the electrical contact resistance in the useful operation conditions [243].

Thermomechanical issues often dictate the choices of electrodes materials and device geometries. Thermoelectric modules consist of many different components such as thermoelements, interconnectors, and packaging enclosures. Thermal expansion mismatch of the materials causes severe stress, leading to the degradation and even breaking of the contacts [244,245]. To prevent the thermal stress, materials with similar thermal expansion coefficients should be chosen. If that is not possible, the thermoelectric module should be designed to minimize those stresses. For example, the T-shunt design [16] may be more durable than a conventional Π-type thermoelectric module under thermal cycles. Proper treatment of the surfaces also can improve interface bonding strength [246,247]. In addition, thermal interface materials based on carbon nanotubes have been under development for better contacts [248,249].

Interconnectors between p-type and n-type pellets are usually made with metals for high electrical and thermal conductivity, but the metal atoms tend to diffuse into the thermoelectric material at high temperature. The diffused metal can change the carrier density and deteriorate the power factor. To prevent the diffusion problem, some metal layers can be used as a diffusion barrier. Therefore, contacts should be designed to satisfy high diffusion barrier, low electrical/thermal contact resistance, and strong interface bonding.

The packaging of thermoelectric modules is also a challenging issue. The reason for the packaging is two-fold: (1) to reduce thermal leakage and (2) to protect thermoelectric modules from harsh environments. Thermal leakage refers to heat transport through void volume in thermoelectric modules, not through thermoelectric pellets, which is already included in *ZT*. Recently, a small filling factor, which is the ratio of a thermoelements area and module area, has been emphasized since material cost can be reduced remarkably [250,251]. In the design with a small filling factor, the thermal leakage becomes more problematic. The heat leaks mostly by radiation and air conduction. Therefore, the thermoelectric pellets need to be coated with low emissivity materials, and vacuum packaging is required. Regarding the second reason for the packaging, protection of thermoelectric modules from harsh environments is important. High temperature operation of thermoelectric modules can cause oxidation of thermoelectric materials, interconnectors, etc. Packaging adds additional challenges in terms of thermomechanical stress, thermal leakage through the rims of the package, electrical insulation, and thermal interfacial resistance between the packaging materials and the thermoelectric modules.

6.2 System Challenges. Application of thermoelectric energy conversion for heat to electricity generation requires careful system design, including both technical and cost considerations. A key advantage of thermoelectric devices is their solid-state nature, which makes them scalable for small power as well as large power applications. The major obstacle for their deployment is low efficiency.

The economics of thermoelectric power generation depend on the nature of the heat source. When developing a thermoelectric system including heat exchangers, heat flux through the

thermoelements should be large enough to maintain the appropriate temperature difference. The typical heat flux through thermoelectric pellets is $\sim 100\,\mathrm{kW/m^2}$, assuming that the pellet thickness is 1 mm and the temperature difference is 100 °C. One can potentially deliver this heat flux by concentrating heat through conduction in the device's hot and cold sides and using fins or any other heat transfer enhancement methods. System optimization is crucial and both the thermoelectric device and the heat exchangers should be developed together to match heat flux through them.

Another issue in thermoelectric system design is varying heat source/sink temperatures over hot/cold sides of the thermoelectric modules. In a typical exhaust waste heat recovery system, heat sink/source (usually fluids) temperature varies along the flow direction. In this case, we can think two limiting cases. The first limiting case is that all the thermoelectric pellets have the same hot/cold side temperature since all the pellets are thermally connected through a highly conductive heat exchanger (e.g., fins). The second limiting case is that all the pellets are thermally isolated from each other and have different hot/cold side temperatures along the flow direction. Thermodynamically, the latter case certainly has much higher system efficiency because temperature difference between the source/sink and hot/cold side of thermoelectric module can be reduced, resulting in less entropy generation. However, to achieve the latter case, there are two major challenges. First, we may need to use different thermoelectric materials along the flow stream since the operating temperature ranges of each thermoelement are different. This probably can be achieved with fine adjustment of carrier concentration. However, if operating temperature ranges are largely different, different types of materials should be used. Second, efficient thermal insulation between thermoelements should be applied. Otherwise, heat leakage through the insulating layer will decrease the efficiency.

Having discussed waste heat applications, we would like to emphasize that thermoelectrics is not limited to waste heat. Thermoelectric energy conversion could also be applied for renewable energy conversion into electricity. In general, thinking about wasted heat availability and entropy generation is probably more appropriate in identifying potential applications. As one example, Kraemer et al. recently developed a solar thermoelectric generator employing a small filling factor to make a large heat flux through thermoelements [251]. Solar insolation is about $1\,\mathrm{kW/m^2}$, which is smaller than the preferred heat flux in thermoelectrics by a factor of 100–200. By using the small filling factor, they could achieve a large temperature gradient and a respectable efficiency. When such solar-thermoelectric generators are combined with solar hot-water systems as the topping cycle, entropy generation is reduced and economics becomes favorable [252].

Regarding the cost issue, which holds the key to deployment of thermoelectric technology, one should keep in mind that other components in the system like heat exchangers can be a significant portion of the system cost. One interesting feature of thermoelectrics is that output power does not depend on the amount of thermoelectric materials used. For example, a thermoelectric pellet with a small area and short length can generate the same amount of electricity as a thermoelectric pellet with a large area and long length if their thermal and electrical resistances are the same. Therefore, material cost can be greatly reduced by reducing both filling factor and thermoelement length [250,251]. For example, according to a recent analysis on solar thermoelectric generators, the material cost can be reduced down to \$0.03/Wp [252]. Then, the major part of the system cost is due to heat exchangers and other balance-of-plant parts.

We hope that the above discussions illustrate that ample room exists in device fabrication and system innovation. The heat transfer community is well poised to make a difference in this area.

7 Conclusion

This review has described the current progress and challenges surrounding heat transfer in thermoelectric materials and devices, with a special focus on heat transfer physics. One primary strategy to boost ZT is to effectively suppress the lattice thermal conductivity without sacrificing electronic properties because the phononic contribution can be controlled relatively independently without power factor deterioration due to the different MFPs between phonons and electrons. Remarkable progress has been made to push down the lattice thermal conductivity. In bulk materials, the efforts have focused on alloying and using phonon rattlers and complex structures. In nanostructured materials, the increased phonon-boundary or phonon-interface scattering has led to dramatic suppression of thermal conductivity. The excellent progress on first-principle calculations has advanced our fundamental understanding of phonon transport physics in bulk materials, which can be used as guidance to further reduce thermal conductivity. The experimental work on nanostructure materials has moved forward rapidly along with the growing nanostructured material syntheses and measurement techniques.

Despite the excellent progress, there are still many remaining questions and challenges. One big problem on the experimental side lies in the difficulty and complexity of experimental systems, from microfabricated platforms to optical systems, which prevent most interested groups from entering the fields and limit the reproducibility of experimental data. One major theoretical challenge is the accurate multiscale phonon modeling of nanocomposites since our understanding of phonon-interface scattering is still limited despite encouraging progress on the calculation of mode-dependent phonon interface transmission. Simulation tools for defects and their impact on phonon transport are still lacking. Device fabrication proceeds slowly due to complexity and system-level heat transfer issues. Better and more innovative design based on heat transfer physics to raise the efficiency would enable more practical applications. We hope that this review will kindle broader interest in thermoelectrics within the heat transfer community, promote even faster development of thermoelectric materials and devices, and eventually lead thermoelectics to be part of the renewable energy solutions.

Acknowledgment

This work is supported S3TEC, an Energy Frontier Research Center funded by the U.S. Department of Energy, Office of Science, Office of Basic Energy Sciences under Award No. DE-FG02-09ER46577 (Z. T. T. and G. C. for power generation), and OSU MURI under Award No. RF01224242 (S. Y. L. for cryogenic refrigeration).

Nomenclature

k_B = Boltzmann constant, $1.38 \times 10^{-23}\,\mathrm{m^2\,kgs^{-2}}$
$\hbar$ = reduced Planck constant, $1.055 \times 10^{-34}\,\mathrm{Js}$
C = spectral volumetric specific heat, $\mathrm{J\,m^{-3}\,Hz^{-1}\,K^{-1}}$
D = density of states per unit volume per unit frequency interval, $\mathrm{m^{-3}\,Hz^{-1}}$
f_{BE} = Bose–Einstein distribution
L = Lorenz number, $\mathrm{W\,\Omega\,K^{-2}}$
S = Seebeck coefficient, $\mathrm{V\,K^{-1}}$
T = temperature, K
v = velocity, $\mathrm{m\,s^{-1}}$
Z = figure of merit, $\mathrm{K^{-1}}$
κ = thermal conductivity, $\mathrm{W\,m^{-1}\,K^{-1}}$
σ = electrical conductivity, $\mathrm{\Omega^{-1}\,m^{-1}}$
τ = lifetime, s
ω = angular frequency, rad · Hz
AMM = acoustic mismatch model
BTE = Boltzmann transport equation
COP = coefficient of performance
DFT = density functional theory
DMM = diffuse mismatch model
EMA = effective medium approach

EMD = equilibrium molecular dynamics
MC = Monte Carlo
MD = molecular dynamics
MFP = mean free path
NEMD = nonequilibrium molecular dynamics
PGEC = phonon-glass electron-crystal

References

[1] Goldsmid, H. J., 2010, *Introduction to Thermoelectricity*, Springer, New York.
[2] Sootsman, J. R., Chung, D. Y., and Kanatzidis, M. G., 2009, "New and Old Concepts in Thermoelectric Materials," Angew. Chem., Int. Ed., **48**(46), pp. 8616–8639.
[3] Slack, G. A., 1995, "New Materials and Performance Limits for Thermoelectric Cooling," *CRC Handbook of Thermoelectrics*, D. M. Rowe, ed., CRC Press, Boca Raton, FL, pp. 407–440.
[4] Mahan, G. D., and Sofo, J. O., 1996, "The Best Thermoelectric," Proc. Natl. Acad. Sci. USA, **93**(15), pp. 7436–7439.
[5] Hicks, L. D., and Dresselhaus, M. S., 1993, "Effect of Quantum-Well Structures on the Thermoelectric Figure of Merit," Phys. Rev. B, **47**(19), pp. 12727–12731.
[6] Hicks, L. D., and Dresselhaus, M. S., 1993, "Thermoelectric Figure of Merit of a One-Dimensional Conductor," Phys. Rev. B, **47**(24), pp. 16631–16634.
[7] Chen, G., Dresselhaus, M. S., Dresselhaus, G., Fleurial, J. P., and Caillat, T., 2003, "Recent Developments in Thermoelectric Materials," Int. Mater. Rev., **48**(1), pp. 45–66.
[8] Minnich, A. J., Dresselhaus, M. S., Ren, Z. F., and Chen, G., 2009, "Bulk Nanostructured Thermoelectric Materials: Current Research and Future Prospects," Energy Environ. Sci., **2**(5), pp. 466–479.
[9] Lan, Y. C., Minnich, A. J., Chen, G., and Ren, Z. F., 2010, "Enhancement of Thermoelectric Figure-of-Merit by a Bulk Nanostructuring Approach," Adv. Funct. Mater., **20**(3), pp. 357–376.
[10] Zebarjadi, M., Esfarjani, K., Dresselhaus, M. S., Ren, Z. F., and Chen, G., 2012, "Perspectives on Thermoelectrics: From Fundamentals to Device Applications," Energy Environ. Sci., **5**(1), pp. 5147–5162.
[11] Wood, C., 1988, "Materials for Thermoelectric Energy Conversion," Rep. Prog. Phys., **51**(4), pp. 459–539.
[12] Snyder, G. J., and Toberer, E. S., 2008, "Complex Thermoelectric Materials," Nature Mater., **7**(2), pp. 105–114.
[13] Dresselhaus, M. S., Chen, G., Tang, M. Y., Yang, R. G., Lee, H., Wang, D. Z., Ren, Z. F., Fleurial, J. P., and Gogna, P., 2007, "New Directions for Low-Dimensional Thermoelectric Materials," Adv. Mater., **19**(8), pp. 1043–1053.
[14] Vineis, C. J., Shakouri, A., Majumdar, A., and Kanatzidis, M. G., 2010, "Nanostructured Thermoelectrics: Big Efficiency Gains From Small Features," Adv. Mater., **22**(36), pp. 3970–3980.
[15] Disalvo, F. J., 1999, "Thermoelectric Cooling and Power Generation," Science, **285**(5428), pp. 703–706.
[16] Bell, L. E., 2008, "Cooling, Heating, Generating Power, and Recovering Waste Heat With Thermoelectric Systems," Science, **321**(5895), pp. 1457–1461.
[17] Chen, G., and Shakouri, A., 2002, "Heat Transfer in Nanostructures for Solid-State Energy Conversion," ASME J. Heat Transfer, **124**(2), pp. 242–252.
[18] Rowe, D. M., 1995, *CRC Handbook of Thermoelectrics*, CRC Press, Boca Raton, FL.
[19] Rowe, D. M., 2006, *Thermoelectrics Handbook: Macro to Nano*, CRC Press, Boca Raton, FL.
[20] Tritt, T. M., 2001, *Recent Trends in Thermoelectric Materials Research, Semiconductors and Semimetals*, Academic Press, San Diego, CA.
[21] Chen, G., 2006, "Nanoscale Heat Transfer and Nanostructured Thermoelectrics," IEEE Trans. Compon. Packag. Technol., **29**(2), pp. 238–246.
[22] Tritt, T. M., and Subramanian, M. A., 2006, "Thermoelectric Materials, Phenomena, and Applications: A Bird's Eye View," MRS Bull., **31**(3), pp. 188–194.
[23] Goldsmid, H. J., and Douglas, R. W., 1954, "The Use of Semiconductors in Thermoelectric Refrigeration," Br. J. Appl. Phys., **5**, pp. 386–390.
[24] Ioffe, A. F., 1957, *Semiconductor Thermoelements and Thermo-Electric Cooling*, Infosearch Ltd., London.
[25] Steele, M. C., and Rosi, F. D., 1958, "Thermal Conductivity and Thermoelectric Power of Germanium-Silicon Alloys," J. Appl. Phys., **29**(11), pp. 1517–1520.
[26] Ioffe, A. F., Airapetiants, S. V., Ioffe, A. V., Kolomoetz, N. V., and Stilbans, L. S., 1956, "Increasing the Efficiency of Semiconductor Thermocouples," Dokl. Akad. Nauk SSSR, **106**(6), p. 981.
[27] Venkatasubramanian, R., Siivola, E., Colpitts, T., and O'Quinn, B., 2001, "Thin-Film Thermoelectric Devices With High Room-Temperature Figures of Merit," Nature, **413**(6856), pp. 597–602.
[28] Shakouri, A., and Bowers, J. E., 1997, "Heterostructure Integrated Thermionic Coolers," Appl. Phys. Lett., **71**(9), pp. 1234–1236.
[29] Zhang, Q., Cao, F., Liu, W. S., Lukas, K., Yu, B., Chen, S., Opeil, C., Broido, D., Chen, G., and Ren, Z. F., 2012, "Heavy Doping and Band Engineering by Potassium to Improve the Thermoelectric Figure of Merit in p-Type PbTe, PbSe, and $PbTe_{1-y}Se_y$," J. Am. Chem. Soc., **134**(24), pp. 10031–10038.
[30] Pei, Y. Z., Shi, X. Y., Lalonde, A., Wang, H., Chen, L. D., and Snyder, G. J., 2011, "Convergence of Electronic Bands for High Performance Bulk Thermoelectrics," Nature, **473**(7345), pp. 66–69.
[31] Biswas, K., He, J., Blum, I. D., Wu, C.-I., Hogan, T. P., Seidman, D. N., Dravid, V. P., and Kanatzidis, M. G., 2012, "High-Performance Bulk Thermoelectrics With All-Scale Hierarchical Architectures," Nature, **489**, pp. 414–418.
[32] Wang, X. W., Lee, H., Lan, Y. C., Zhu, G. H., Joshi, G., Wang, D. Z., Yang, J., Muto, A. J., Tang, M. Y., Klatsky, J., Song, S., Dresselhaus, M. S., Chen, G., and Ren, Z. F., 2008, "Enhanced Thermoelectric Figure of Merit in Nanostructured n-Type Silicon Germanium Bulk Alloy," Appl. Phys. Lett., **93**(19), p. 193121.
[33] Joshi, G., Lee, H., Lan, Y. C., Wang, X. W., Zhu, G. H., Wang, D. Z., Gould, R. W., Cuff, D. C., Tang, M. Y., Dresselhaus, M. S., Chen, G., and Ren, Z. F., 2008, "Enhanced Thermoelectric Figure-of-Merit in Nanostructured p-Type Silicon Germanium Bulk Alloys," Nano Lett., **8**(12), pp. 4670–4674.
[34] Uher, C., 2001, "Skutterudites: Prospective Novel Thermoelectrics," Semicond. Semimetals, **69**, pp. 139–253.
[35] Nolas, G. S., Slack, G. A., Morelli, D. T., Tritt, T. M., and Ehrlich, A. C., 1996, "The Effect of Rare-Earth Filling on the Lattice Thermal Conductivity of Skutterudites," J. Appl. Phys., **79**(8), pp. 4002–4008.
[36] Sales, B. C., Mandrus, D., and Williams, R. K., 1996, "Filled Skutterudite Antimonides: A New Class of Thermoelectric Materials," Science, **272**(5266), pp. 1325–1328.
[37] Morelli, D. T., Meisner, G. P., Chen, B. X., Hu, S. Q., and Uher, C., 1997, "Cerium Filling and Doping of Cobalt Triantimonide," Phys. Rev. B, **56**(12), pp. 7376–7383.
[38] Shi, X., Kong, H., Li, C. P., Uher, C., Yang, J., Salvador, J. R., Wang, H., Chen, L., and Zhang, W., 2008, "Low Thermal Conductivity and High Thermoelectric Figure of Merit in n-Type $Ba_xYb_yCo_4Sb_{12}$ Double-Filled Skutterudites," Appl. Phys. Lett., **92**(18), p. 182101.
[39] Shi, X., Yang, J., Salvador, J. R., Chi, M. F., Cho, J. Y., Wang, H., Bai, S. Q., Yang, J. H., Zhang, W. Q., and Chen, L. D., 2011, "Multiple-Filled Skutterudites: High Thermoelectric Figure of Merit Through Separately Optimizing Electrical and Thermal Transports," J. Am. Chem. Soc., **133**(20), pp. 7837–7846.
[40] Jie, Q., Wang, H., Liu, W., Wang, H., Chen, G., and Ren, Z., "Fast Phase Formation of Double-Filled p-Type Skutterudites by Ball-Milling and Hot-Pressing," Phys. Chem. Chem. Phys. (accepted).
[41] Saramat, A., Svensson, G., Palmqvist, A. E. C., Stiewe, C., Mueller, E., Platzek, D., Williams, S. G. K., Rowe, D. M., Bryan, J. D., and Stucky, G. D., 2006, "Large Thermoelectric Figure of Merit at High Temperature in Czochralski-Grown Clathrate $Ba_8Ga_{16}Ge_{30}$," J. Appl. Phys., **99**(2), p. 023708.
[42] Deng, S. K., Tang, X. F., Li, P., and Zhang, Q. J., 2008, "High Temperature Thermoelectric Transport Properties of p-Type $Ba_8Ga_{16}Al_xGe_{30-x}$ Type-I Clathrates With High Performance," J. Appl. Phys., **103**(7), p. 073503.
[43] Caillat, T., Fleurial, J. P., and Borshchevsky, A., 1997, "Preparation and Thermoelectric Properties of Semiconducting Zn_4Sb_3," J. Phys. Chem. Solids, **58**(7), pp. 1119–1125.
[44] Brown, S. R., Kauzlarich, S. M., Gascoin, F., and Snyder, G. J., 2006, "$Yb_{14}MnSb_{11}$: New High Efficiency Thermoelectric Material for Power Generation," Chem. Mater., **18**(7), pp. 1873–1877.
[45] Wolfing, B., Kloc, C., Teubner, J., and Bucher, E., 2001, "High Performance Thermoelectric Tl_9BiTe_6 With an Extremely Low Thermal Conductivity," Phys. Rev. Lett., **86**(19), pp. 4350–4353.
[46] Kurosaki, K., Kosuga, A., Muta, H., and Yamanaka, S., 2005, "Thermoelectric Properties of Thallium Compounds With Extremely Low Thermal Conductivity," Mater. Trans., **46**(7), pp. 1502–1505.
[47] Uher, C., Yang, J., Hu, S., Morelli, D. T., and Meisner, G. P., 1999, "Transport Properties of Pure and Doped MNiSn (M = Zr, Hf)," Phys. Rev. B, **59**(13), pp. 8615–8621.
[48] Yan, X. A., Joshi, G., Liu, W. S., Lan, Y. C., Wang, H., Lee, S., Simonson, J. W., Poon, S. J., Tritt, T. M., Chen, G., and Ren, Z. F., 2011, "Enhanced Thermoelectric Figure of Merit of p-Type Half-Heuslers," Nano Lett., **11**(2), pp. 556–560.
[49] Joshi, G., Yan, X., Wang, H. Z., Liu, W. S., Chen, G., and Ren, Z. F., 2011, "Enhancement in Thermoelectric Figure-of-Merit of an *N*-Type Half-Heusler Compound by the Nanocomposite Approach," Adv. Energy Mater., **1**(4), pp. 643–647.
[50] Yan, X., Liu, W. S., Wang, H., Chen, S., Shiomi, J., Esfarjani, K., Wang, H. Z., Wang, D. Z., Chen, G., and Ren, Z. F., 2012, "Stronger Phonon Scattering by Larger Differences in Atomic Mass and Size in p-Type Half-Heuslers $Hf_{1-x}Ti_xCoSb_{0.8}Sn_{0.2}$," Energy Environ. Sci., **5**(6), pp. 7543–7548.
[51] Terasaki, I., Sasago, Y., and Uchinokura, K., 1997, "Large Thermoelectric Power in $NaCo_2O_4$ Single Crystals," Phys. Rev. B, **56**(20), pp. 12685–12687.
[52] Funahashi, R., Matsubara, I., Ikuta, H., Takeuchi, T., Mizutani, U., and Sodeoka, S., 2000, "An Oxide Single Crystal With High Thermoelectric Performance in Air," Jpn. J. Appl. Phys., Part 2, **39**(11B), pp. L1127–L1129.
[53] Funahashi, R., Matsubara, I., and Sodeoka, S., 2000, "Thermoelectric Properties of $Bi_2Sr_2Co_2O_x$ Polycrystalline Materials," Appl. Phys. Lett., **76**(17), pp. 2385–2387.
[54] Ohta, S., Nomura, T., Ohta, H., and Koumoto, K., 2005, "High-Temperature Carrier Transport and Thermoelectric Properties of Heavily La- or Nb-Doped $SrTiO_3$ Single Crystals," J. Appl. Phys., **97**(3), p. 034106.
[55] Flahaut, D., Mihara, T., Funahashi, R., Nabeshima, N., Lee, K., Ohta, H., and Koumoto, K., 2006, "Thermoelectrical Properties of *A*-Site Substituted $Ca_{1-x}Re_xMnO_3$ System," J. Appl. Phys., **100**(8), p. 084911.
[56] Muta, H., Kurosaki, K., and Yamanaka, S., 2003, "Thermoelectric Properties of Rare Earth Doped $SrTiO_3$," J. Alloys Compd., **350**(1–2), pp. 292–295.
[57] Zhou, J., Yang, R. G., Chen, G., and Dresselhaus, M. S., 2011, "Optimal Bandwidth for High Efficiency Thermoelectrics," Phys. Rev. Lett., **107**(22), p. 226601.

[58] Jeong, C., Kim, R., and Lundstrom, M. S., 2012, "On the Best Bandstructure for Thermoelectric Performance: A Landauer Perspective," J. Appl. Phys., **111**(11), p. 113707.
[59] Heremans, J. P., Jovovic, V., Toberer, E. S., Saramat, A., Kurosaki, K., Charoenphakdee, A., Yamanaka, S., and Snyder, G. J., 2008, "Enhancement of Thermoelectric Efficiency in PbTe by Distortion of the Electronic Density of States," Science, **321**(5888), pp. 554–557.
[60] Zhang, Q. Y., Wang, H., Liu, W. S., Wang, H. Z., Yu, B., Zhang, Q., Tian, Z. T., Ni, G., Lee, S., Esfarjani, K., Chen, G., and Ren, Z. F., 2012, "Enhancement of Thermoelectric Figure-of-Merit by Resonant States of Aluminium Doping in Lead Selenide," Energy Environ. Sci., **5**(1), pp. 5246–5251.
[61] Heremans, J. P., Thrush, C. M., and Morelli, D. T., 2004, "Thermopower Enhancement in Lead Telluride Nanostructures," Phys. Rev. B, **70**(11), p. 115334.
[62] Zide, J. M. O., Vashaee, D., Bian, Z. X., Zeng, G., Bowers, J. E., Shakouri, A., and Gossard, A. C., 2006, "Demonstration of Electron Filtering to Increase the Seebeck Coefficient in $In_{0.53}Ga_{0.47}As/In_{0.53}Ga_{0.28}Al_{0.19}As$ Superlattices," Phys. Rev. B, **74**(20), p. 205335.
[63] Zebarjadi, M., Joshi, G., Zhu, G. H., Yu, B., Minnich, A., Lan, Y. C., Wang, X. W., Dresselhaus, M., Ren, Z. F., and Chen, G., 2011, "Power Factor Enhancement by Modulation Doping in Bulk Nanocomposites," Nano Lett., **11**(6), pp. 2225–2230.
[64] Koga, T., Sun, X., Cronin, S. B., and Dresselhaus, M. S., 1998, "Carrier Pocket Engineering to Design Superior Thermoelectric Materials Using GaAs/AlAs Superlattices," Appl. Phys. Lett., **73**(20), pp. 2950–2952.
[65] Zebarjadi, M., Liao, B., Esfarjani, K., Dresselhaus, M., and Chen, G., 2013, "Enhancing the Thermoelectric Power Factor by Using Invisible Dopants," Adv. Mater., **25**(11), pp. 1577–1582.
[66] Chen, G., Tien, C. L., Wu, X., and Smith, J. S., 1994, "Thermal Diffusivity Measurement of GaAs/AlGaAs Thin-Film Structures," ASME J. Heat Transfer, **116**(2), pp. 325–331.
[67] Chen, G., 2001, "Phonon Transport in Low-Dimensional Structures," Semicond. Semimetals, **71**, pp. 203–259.
[68] Harman, T. C., Taylor, P. J., Walsh, M. P., and Laforge, B. E., 2002, "Quantum Dot Superlattice Thermoelectric Materials and Devices," Science, **297**(5590), pp. 2229–2232.
[69] Lee, S. M., Cahill, D. G., and Venkatasubramanian, R., 1997, "Thermal Conductivity of Si-Ge Superlattices," Appl. Phys. Lett., **70**(22), pp. 2957–2959.
[70] Liu, W. L., Borca-Tasciuc, T., Chen, G., Liu, J. L., and Wang, K. L., 2001, "Anisotropic Thermal Conductivity of Ge Quantum-Dot and Symmetrically Strained Si/Ge Superlattices," J. Nanosci. Nanotechnol., **1**(1), pp. 39–42.
[71] Borca-Tasciuc, T., Liu, W. L., Liu, J. L., Zeng, T. F., Song, D. W., Moore, C. D., Chen, G., Wang, K. L., Goorsky, M. S., Radetic, T., Gronsky, R., Koga, T., and Dresselhaus, M. S., 2000, "Thermal Conductivity of Symmetrically Strained Si/Ge Superlattices," Superlattices Microstruct., **28**(3), pp. 199–206.
[72] Capinski, W. S., Maris, H. J., Ruf, T., Cardona, M., Ploog, K., and Katzer, D. S., 1999, "Thermal-Conductivity Measurements of GaAs/AlAs Superlattices Using a Picosecond Optical Pump-And-Probe Technique," Phys. Rev. B, **59**(12), pp. 8105–8113.
[73] Caylor, J. C., Coonley, K., Stuart, J., Colpitts, T., and Venkatasubramanian, R., 2005, "Enhanced Thermoelectric Performance in PbTe-Based Superlattice Structures From Reduction of Lattice Thermal Conductivity," Appl. Phys. Lett., **87**(2), p. 023105.
[74] Heremans, J., Thrush, C. M., Lin, Y. M., Cronin, S., Zhang, Z., Dresselhaus, M. S., and Mansfield, J. F., 2000, "Bismuth Nanowire Arrays: Synthesis and Galvanomagnetic Properties," Phys. Rev. B, **61**(4), pp. 2921–2930.
[75] Guthy, C., Nam, C. Y., and Fischer, J. E., 2008, "Unusually Low Thermal Conductivity of Gallium Nitride Nanowires," J. Appl. Phys., **103**(6), p. 064319.
[76] Harris, C. T., Martinez, J. A., Shaner, E. A., Huang, J. Y., Swartzentruber, B. S., Sullivan, J. P., and Chen, G., 2011, "Fabrication of a Nanostructure Thermal Property Measurement Platform," Nanotechnology, **22**(27), p. 275308.
[77] Zhou, J. H., Jin, C. G., Seol, J. H., Li, X. G., and Shi, L., 2005, "Thermoelectric Properties of Individual Electrodeposited Bismuth Telluride Nanowires," Appl. Phys. Lett., **87**(13), p. 133109.
[78] Zhou, F., Moore, A. L., Pettes, M. T., Lee, Y., Seol, J. H., Ye, Q. L., Rabenberg, L., and Shi, L., 2010, "Effect of Growth Base Pressure on the Thermoelectric Properties of Indium Antimonide Nanowires," J. Phys. D: Appl. Phys., **43**(2), p. 025406.
[79] Zhou, F., Moore, A. L., Bolinsson, J., Persson, A., Froberg, L., Pettes, M. T., Kong, H. J., Rabenberg, L., Caroff, P., Stewart, D. A., Mingo, N., Dick, K. A., Samuelson, L., Linke, H., and Shi, L., 2011, "Thermal Conductivity of Indium Arsenide Nanowires With Wurtzite and Zinc Blende Phases," Phys. Rev. B, **83**(20), p. 205416.
[80] Moore, A. L., Pettes, M. T., Zhou, F., and Shi, L., 2009, "Thermal Conductivity Suppression in Bismuth Nanowires," J. Appl. Phys., **106**(3), p. 034310.
[81] Hochbaum, A. I., Chen, R. K., Delgado, R. D., Liang, W. J., Garnett, E. C., Najarian, M., Majumdar, A., and Yang, P. D., 2008, "Enhanced Thermoelectric Performance of Rough Silicon Nanowires," Nature, **451**(7175), pp. 163–167.
[82] Boukai, A. I., Bunimovich, Y., Tahir-Kheli, J., Yu, J. K., Goddard, W. A., and Heath, J. R., 2008, "Silicon Nanowires as Efficient Thermoelectric Materials," Nature, **451**(7175), pp. 168–171.
[83] Wingert, M. C., Chen, Z. C. Y., Dechaumphai, E., Moon, J., Kim, J. H., Xiang, J., and Chen, R. K., 2011, "Thermal Conductivity of Ge and Ge-Si Core-Shell Nanowires in the Phonon Confinement Regime," Nano Lett., **11**(12), pp. 5507–5513.
[84] Lee, E. K., Yin, L., Lee, Y., Lee, J. W., Lee, S. J., Lee, J., Cha, S. N., Whang, D., Hwang, G. S., Hippalgaonkar, K., Majumdar, A., Yu, C., Choi, B. L., Kim, J. M., and Kim, K., 2012, "Large Thermoelectric Figure-of-Merits From SiGe Nanowires by Simultaneously Measuring Electrical and Thermal Transport Properties," Nano Lett., **12**(6), pp. 2918–2923.
[85] Zhao, X. B., Ji, X. H., Zhang, Y. H., Zhu, T. J., Tu, J. P., and Zhang, X. B., 2005, "Bismuth Telluride Nanotubes and the Effects on the Thermoelectric Properties of Nanotube-Containing Nanocomposites," Appl. Phys. Lett., **86**(6), p. 062111.
[86] Yang, R., and Chen, G., 2004, "Thermal Conductivity Modeling of Periodic Two-Dimensional Nanocomposites," Phys. Rev. B, **69**(19), p. 195316.
[87] Lan, Y. C., Poudel, B., Ma, Y., Wang, D. Z., Dresselhaus, M. S., Chen, G., and Ren, Z. F., 2009, "Structure Study of Bulk Nanograined Thermoelectric Bismuth Antimony Telluride," Nano Lett., **9**(4), pp. 1419–1422.
[88] Poudel, B., Hao, Q., Ma, Y., Lan, Y. C., Minnich, A., Yu, B., Yan, X. A., Wang, D. Z., Muto, A., Vashaee, D., Chen, X. Y., Liu, J. M., Dresselhaus, M. S., Chen, G., and Ren, Z. F., 2008, "High-Thermoelectric Performance of Nanostructured Bismuth Antimony Telluride Bulk Alloys," Science, **320**(5876), pp. 634–638.
[89] Ma, Y., Hao, Q., Poudel, B., Lan, Y. C., Yu, B., Wang, D. Z., Chen, G., and Ren, Z. F., 2008, "Enhanced Thermoelectric Figure-of-Merit in p-Type Nanostructured Bismuth Antimony Tellurium Alloys Made From Elemental Chunks," Nano Lett., **8**(8), pp. 2580–2584.
[90] Girard, S. N., He, J. Q., Zhou, X. Y., Shoemaker, D., Jaworski, C. M., Uher, C., Dravid, V. P., Heremans, J. P., and Kanatzidis, M. G., 2011, "High Performance Na-Doped PbTe-PbS Thermoelectric Materials: Electronic Density of States Modification and Shape-Controlled Nanostructures," J. Am. Chem. Soc., **133**(41), pp. 16588–16597.
[91] Poudeu, P. F. P., D'Angelo, J., Downey, A. D., Short, J. L., Hogan, T. P., and Kanatzidis, M. G., 2006, "High Thermoelectric Figure of Merit and Nanostructuring in Bulk p-Type $Na_{1-x}Pb_mSb_yTe_{m+2}$," Angew. Chem., Int. Ed., **45**(23), pp. 3835–3839.
[92] Kim, W., Zide, J., Gossard, A., Klenov, D., Stemmer, S., Shakouri, A., and Majumdar, A., 2006, "Thermal Conductivity Reduction and Thermoelectric Figure of Merit Increase by Embedding Nanoparticles in Crystalline Semiconductors," Phys. Rev. Lett., **96**(4), p. 045901.
[93] Ge, Z. H., Zhang, B. P., Liu, Y., and Li, J. F., 2012, "Nanostructured $Bi_{2-x}Cu_xS_3$ Bulk Materials With Enhanced Thermoelectric Performance," Phys. Chem. Chem. Phys., **14**(13), pp. 4475–4481.
[94] Li, H., Tang, X., Zhang, Q., and Uher, C., 2008, "Rapid Preparation Method of Bulk Nanostructured $Yb_{0.3}Co_4Sb_{12+y}$ Compounds and Their Improved Thermoelectric Performance," Appl. Phys. Lett., **93**(25), p. 252109.
[95] Li, H., Tang, X., Zhang, Q., and Uher, C., 2009, "High Performance $In_xCe_yCo_4Sb_{12}$ Thermoelectric Materials With *in situ* Forming Nanostructured InSb Phase," Appl. Phys. Lett., **94**(10), p. 102114.
[96] Yan, X., Poudel, B., Ma, Y., Liu, W. S., Joshi, G., Wang, H., Lan, Y. C., Wang, D. Z., Chen, G., and Ren, Z. F., 2010, "Experimental Studies on Anisotropic Thermoelectric Properties and Structures of n-Type $Bi_2Te_{2.7}Se_{0.3}$," Nano Lett., **10**(9), pp. 3373–3378.
[97] Peierls, R., 1929, "The Kinetic Theory of Thermal Conduction in Crystals," Ann. Phys., **3**(8), pp. 1055–1101.
[98] Callaway, J., 1959, "Model for Lattice Thermal Conductivity at Low Temperatures," Phys. Rev., **113**(4), pp. 1046–1051.
[99] Klemens, P. G., 1958, "Thermal Conductivity and Lattice Vibrational Modes," Solid State Phys., Adv. Res. Appl., **7**, pp. 1–98.
[100] Holland, M. G., 1963, "Analysis of Lattice Thermal Conductivity," Phys. Rev., **132**(6), pp. 2461–2471.
[101] de Haas, W. J., and Biermasz, T., 1938, "The Dependence of Thickness of the Thermal Resistance of Crystals at Low Temperatures," Physica, **5**, pp. 619–624.
[102] Casimir, H. B. G., 1938, "Note on the Conduction of Heat in Crystals," Physica, **5**, pp. 495–500.
[103] Ziman, J. M., 1960, *Electrons and Phonons: The Theory of Transport Phenomena in Solids, International Series of Monographs on Physics*, Clarendon Press, Oxford, UK.
[104] Ladd, A. J. C., Moran, B., and Hoover, W. G., 1986, "Lattice Thermal Conductivity—A Comparison of Molecular Dynamics and Anharmonic Lattice Dynamics," Phys. Rev. B, **34**(8), pp. 5058–5064.
[105] Volz, S. G., and Chen, G., 2000, "Molecular-Dynamics Simulation of Thermal Conductivity of Silicon Crystals," Phys. Rev. B, **61**(4), pp. 2651–2656.
[106] Li, J., Porter, L., and Yip, S., 1998, "Atomistic Modeling of Finite-Temperature Properties of Crystalline Beta-SiC: II. Thermal Conductivity and Effects of Point Defects," J. Nucl. Mater., **255**(2–3), pp. 139–152.
[107] Che, J. W., Cagin, T., Deng, W. Q., and Goddard, W. A., 2000, "Thermal Conductivity of Diamond and Related Materials From Molecular Dynamics Simulations," J. Chem. Phys., **113**(16), pp. 6888–6900.
[108] Oligschleger, C., and Schon, J. C., 1999, "Simulation of Thermal Conductivity and Heat Transport in Solids," Phys. Rev. B, **59**(6), pp. 4125–4133.
[109] Green, M. S., 1954, "Markoff Random Processes and the Statistical Mechanics of Time-Dependent Phenomena 2. Irreversible Process in Fluids," J. Chem. Phys., **22**(3), pp. 398–413.
[110] Kubo, R., Yokota, M., and Nakajima, S., 1957, "Statistical Mechanical Theory of Irreversible Processes 2. Response to Thermal Disturbance," J. Phys. Soc. Jpn., **12**(11), pp. 1203–1211.
[111] Hoover, W. G., and Ashurst, W. T., 1975, "Nonequilibrium Molecular Dynamics," Theor. Chem.: Adv. Perspect., **1**, pp. 1–51.
[112] Kotake, S., and Wakuri, S., 1994, "Molecular Dynamics Study of Heat Conduction in Solid Materials," JSME Int. J., Ser. B, **37**(1), pp. 103–108.

[113] Ikeshoji, T., and Hafskjold, B., 1994, "Nonequilibrium Molecular Dynamics Calculations of Heat Conduction in Liquid and Through Liquid-Gas Interface," Mol. Phys., **81**(2), pp. 251–261.
[114] Chen, G., 2005, *Nanoscale Energy Transport and Conversion: A Parallel Treatment of Electrons, Molecules, Phonons, and Photons* (MIT-Pappalardo Series in Mechanical Engineering), Oxford University Press, New York.
[115] Henry, A. S., and Chen, G., 2008, "Spectral Phonon Transport Properties of Silicon Based on Molecular Dynamics Simulations and Lattice Dynamics," J. Comput. Theor. Nanosci., **5**(2), pp. 141–152.
[116] McGaughey, A. J. H., and Kaviany, M., 2004, "Quantitative Validation of the Boltzmann Transport Equation Phonon Thermal Conductivity Model Under the Single-Mode Relaxation Time Approximation," Phys. Rev. B, **69**(9), p. 094303.
[117] Turney, J. E., Landry, E. S., McGaughey, A. J. H., and Amon, C. H., 2009, "Predicting Phonon Properties and Thermal Conductivity From Anharmonic Lattice Dynamics Calculations and Molecular Dynamics Simulations," Phys. Rev. B, **79**(6), p. 064301.
[118] Qiu, B., Bao, H., Zhang, G. Q., Wu, Y., and Ruan, X. L., 2012, "Molecular Dynamics Simulations of Lattice Thermal Conductivity and Spectral Phonon Mean Free Path of PbTe: Bulk and Nanostructures," Comput. Mater. Sci., **53**(1), pp. 278–285.
[119] Broido, D. A., Ward, A., and Mingo, N., 2005, "Lattice Thermal Conductivity of Silicon From Empirical Interatomic Potentials," Phys. Rev. B, **72**(1), p. 014308.
[120] Tuckerman, M. E., 2002, "Ab Initio Molecular Dynamics: Basic Concepts, Current Trends and Novel Applications," J. Phys.: Condens. Matter, **14**(50), pp. R1297–R1355.
[121] Kim, H., and Kaviany, M., 2012, "Effect of Thermal Disorder on High Figure of Merit in PbTe," Phys. Rev. B, **86**(4), p. 045213.
[122] Broido, D., Malorny, M., Birner, G., Mingo, N., and Stewart, D., 2007, "Intrinsic Lattice Thermal Conductivity of Semiconductors From First Principles," Appl. Phys. Lett., **91**(23), p. 231922.
[123] Deinzer, G., Birner, G., and Strauch, D., 2003, "Ab Initio Calculation of the Linewidth of Various Phonon Modes in Germanium and Silicon," Phys. Rev. B, **67**(14), p. 144304.
[124] Esfarjani, K., and Stokes, H., 2008, "Method to Extract Anharmonic Force Constants From First Principles Calculations," Phys. Rev. B, **77**(14), p. 144112.
[125] Esfarjani, K., Chen, G., and Stokes, H., 2011, "Heat Transport in Silicon From First-Principles Calculations," Phys. Rev. B, **84**(8), p. 085204.
[126] Garg, J., Bonini, N., Kozinsky, B., and Marzari, N., 2011, "Role of Disorder and Anharmonicity in the Thermal Conductivity of Silicon-Germanium Alloys: A First-Principles Study," Phys. Rev. Lett., **106**(4), p. 045901.
[127] Garg, J., Bonini, N., and Marzari, N., 2011, "High Thermal Conductivity in Short-Period Superlattices," Nano Lett., **11**(12), pp. 5135–5141.
[128] Tian, Z., Garg, J., Esfarjani, K., Shiga, T., Shiomi, J., and Chen, G., 2012, "Phonon Conduction in PbSe, PbTe, and $PbTe_{1-x}Se_x$ From First-Principles Calculations," Phys. Rev. B, **85**(18), p. 184303.
[129] Shiomi, J., Esfarjani, K., and Chen, G., 2011, "Thermal Conductivity of Half-Heusler Compounds From First-Principles Calculations," Phys. Rev. B, **84**(10), p. 104302.
[130] Shiga, T., Shiomi, J., Ma, J., Delaire, O., Radzynski, T., Lusakowski, A., Esfarjani, K., and Chen, G., 2012, "Microscopic Mechanism of Low Thermal Conductivity in Lead Telluride," Phys. Rev. B, **85**(15), p. 155203.
[131] Luo, T., Garg, J., Shiomi, J., Esfarjani, K., and Chen, G., 2013, "Gallium Arsenide Thermal Conductivity and Optical Phonon Relaxation Times From First-Principles Calculations," Europhys. Lett., **101**, p. 16001.
[132] Minnich, A. J., Johnson, J. A., Schmidt, A. J., Esfarjani, K., Dresselhaus, M. S., Nelson, K. A., and Chen, G., 2011, "Thermal Conductivity Spectroscopy Technique to Measure Phonon Mean Free Paths," Phys. Rev. Lett., **107**(9), p. 095901.
[133] Lee, S., Esfarjani, K., Garg, J., and Chen, G., "Lattice Thermal Transport in Bi, Sb, and Bi-Sb Alloy From First Principles," (unsubmitted manuscript).
[134] Bergman, L., Alexson, D., Murphy, P. L., Nemanich, R. J., Dutta, M., Stroscio, M. A., Balkas, C., Shin, H., and Davis, R. F., 1999, "Raman Analysis of Phonon Lifetimes in AlN and GaN of Wurtzite Structure," Phys. Rev. B, **59**(20), pp. 12977–12982.
[135] Letcher, J. J., Kang, K., Cahill, D. G., and Dlott, D. D., 2007, "Effects of High Carrier Densities on Phonon and Carrier Lifetimes in Si by Time-Resolved Anti-Stokes Raman Scattering," Appl. Phys. Lett., **90**(25), p. 252104.
[136] Delaire, O., Ma, J., Marty, K., May, A. F., McGuire, M. A., Du, M. H., Singh, D. J., Podlesnyak, A., Ehlers, G., Lumsden, M. D., and Sales, B. C., 2011, "Giant Anharmonic Phonon Scattering in PbTe," Nature Mater., **10**(8), pp. 614–619.
[137] Hoesch, M., Fukuda, T., Mizuki, J., Takenouchi, T., Kawarada, H., Sutter, J. P., Tsutsui, S., Baron, A. Q. R., Nagao, M., and Takano, Y., 2007, "Phonon Softening in Superconducting Diamond," Phys. Rev. B, **75**(14), p. 140508.
[138] Dames, C., and Chen, G., 2006, "Thermal Conductivity of Nanostructured Thermoelectric Materials," *Thermoelectrics Handbook: Macro to Nano*, D. M. Rowe, ed., CRC Press, Boca Raton, FL, Chap. 42.
[139] Koh, Y. K., and Cahill, D. G., 2007, "Frequency Dependence of the Thermal Conductivity of Semiconductor Alloys," Phys. Rev. B, **76**(7), p. 075207.
[140] Minnich, A. J., Chen, G., Mansoor, S., and Yilbas, B. S., 2011, "Quasiballistic Heat Transfer Studied Using the Frequency-Dependent Boltzmann Transport Equation," Phys. Rev. B, **84**(23), p. 235207.
[141] Chen, G., 1996, "Nonlocal and Nonequilibrium Heat Conduction in the Vicinity of Nanoparticles," ASME J. Heat Transfer, **118**(3), pp. 539–545.
[142] Siemens, M. E., Li, Q., Yang, R. G., Nelson, K. A., Anderson, E. H., Murnane, M. M., and Kapteyn, H. C., 2010, "Quasi-Ballistic Thermal Transport From Nanoscale Interfaces Observed Using Ultrafast Coherent Soft X-Ray Beams," Nature Mater., **9**(1), pp. 26–30.
[143] Johnson, J. A., Maznev, A. A., Eliason, J. K., Minnich, A., Collins, K., Chen, G., Cuffe, J., Kehoe, T., Sotomayor Torres, C. M., and Nelson, K. A., 2011, "Experimental Evidence of Non-Diffusive Thermal Transport in Si and GaAs," MRS Proc., **1347**, Paper No. mrss11-1347-bb08-03.
[144] Minnich, A. J., 2012, "Determining Phonon Mean Free Paths From Observations of Quasiballistic Thermal Transport," Phys. Rev. Lett., **109**(20), p. 205901.
[145] Humphrey, T. E., and Linke, H., 2005, "Reversible Thermoelectric Nanomaterials," Phys. Rev. Lett., **94**(9), p. 096601.
[146] Flage-Larsen, E., and Prytz, O., 2011, "The Lorenz Function: Its Properties at Optimum Thermoelectric Figure-of-Merit," Appl. Phys. Lett., **99**(20), p. 202108.
[147] Kaibe, H., Tanaka, Y., Sakata, M., and Nishida, I., 1989, "Anisotropic Galvanomagnetic and Thermoelectric Properties of n-Type Bi_2Te_3 Single-Crystal With the Composition of a Useful Thermoelectric Cooling Material," J. Phys. Chem. Solids, **50**(9), pp. 945–950.
[148] Gallo, C. F., Chandrasekhar, B. S., and Sutter, P. H., 1963, "Transport Properties of Bismuth Single Crystals," J. Appl. Phys., **34**(1), pp. 144–152.
[149] White, G. K., and Woods, S. B., 1958, "The Thermal and Electrical Resistivity of Bismuth and Antimony at Low Temperatures," Philos. Mag., **3**(28), pp. 342–359.
[150] Uher, C., and Goldsmid, H. J., 1974, "Separation of the Electronic and Lattice Thermal Conductivities in Bismuth Crystals," Phys. Status Solidi, **65**(2), pp. 765–772.
[151] Abeles, B., 1963, "Lattice Thermal Conductivity of Disordered Semiconductor Alloys at High Temperatures," Phys. Rev., **131**(5), pp. 1906–1911.
[152] Klemens, P. G., 1955, "The Scattering of Low-Frequency Lattice Waves by Static Imperfections," Proc. Phys. Soc. London, Sect. A, **68**(12), pp. 1113–1128.
[153] Tamura, S., 1983, "Isotope Scattering of Dispersive Phonons in Ge," Phys. Rev. B, **27**(2), pp. 858–866.
[154] Klemens, P. G., 1960, "Thermal Resistance Due to Point Defects at High Temperatures," Phys. Rev., **119**(2), pp. 507–509.
[155] Anderson, P. W., 1958, "Absence of Diffusion in Certain Random Lattices," Phys. Rev., **109**(5), pp. 1492–1505.
[156] Mott, N. F., 1968, "Metal-Insulator Transition," Rev. Mod. Phys., **40**(4), pp. 677–683.
[157] Sales, B. C., Mandrus, D., Chakoumakos, B. C., Keppens, V., and Thompson, J. R., 1997, "Filled Skutterudite Antimonides: Electron Crystals and Phonon Glasses," Phys. Rev. B, **56**(23), pp. 15081–15089.
[158] Keppens, V., Mandrus, D., Sales, B. C., Chakoumakos, B. C., Dai, P., Coldea, R., Maple, M. B., Gajewski, D. A., Freeman, E. J., and Bennington, S., 1998, "Localized Vibrational Modes in Metallic Solids," Nature, **395**(6705), pp. 876–878.
[159] Long, G. J., Hermann, R. P., Grandjean, F., Alp, E. E., Sturhahn, W., Johnson, C. E., Brown, D. E., Leupold, O., and Ruffer, R., 2005, "Strongly Decoupled Europium and Iron Vibrational Modes in Filled Skutterudites," Phys. Rev. B, **71**(14), p. 140302.
[160] Grannan, E. R., Randeria, M., and Sethna, J. P., 1990, "Low Temperature Properties of A Model Glass 2. Specific Heat and Thermal Transport," Phys. Rev. B, **41**(11), pp. 7799–7821.
[161] Yang, J., Zhang, W., Bai, S. Q., Mei, Z., and Chen, L. D., 2007, "Dual-Frequency Resonant Phonon Scattering in $Ba_xR_yCo_4Sb_{12}$ (R = La, Ce, and Sr)," Appl. Phys. Lett., **90**(19), p. 192111.
[162] Wang, Y. G., Xu, X. F., and Yang, J. H., 2009, "Resonant Oscillation of Misch-Metal Atoms in Filled Skutterudites," Phys. Rev. Lett., **102**(17), p. 175508.
[163] Meisner, G. P., Morelli, D. T., Hu, S., Yang, J., and Uher, C., 1998, "Structure and Lattice Thermal Conductivity of Fractionally Filled Skutterudites: Solid Solutions of Fully Filled and Unfilled End Members," Phys. Rev. Lett., **80**(16), pp. 3551–3554.
[164] Bai, S. Q., Shi, X., and Chen, L. D., 2010, "Lattice Thermal Transport in Ba_x-$RE_yCo_4Sb_{12}$ (RE = Ce, Yb, and Eu) Double-Filled Skutterudites," Appl. Phys. Lett., **96**(20), p. 202102.
[165] Koza, M. M., Johnson, M. R., Viennois, R., Mutka, H., Girard, L., and Ravot, D., 2008, "Breakdown of Phonon Glass Paradigm in La- and Ce-Filled Fe_4Sb_{12} Skutterudites," Nature Mater., **7**(10), pp. 805–810.
[166] Zebarjadi, M., Esfarjani, K., Yang, J. A., Ren, Z. F., and Chen, G., 2010, "Effect of Filler Mass and Binding on Thermal Conductivity of Fully Filled Skutterudites," Phys. Rev. B, **82**(19), p. 195207.
[167] Li, D. Y., Wu, Y. Y., Kim, P., Shi, L., Yang, P. D., and Majumdar, A., 2003, "Thermal Conductivity of Individual Silicon Nanowires," Appl. Phys. Lett., **83**(14), pp. 2934–2936.
[168] Ponomareva, I., Srivastava, D., and Menon, M., 2007, "Thermal Conductivity in Thin Silicon Nanowires: Phonon Confinement Effect," Nano Lett., **7**(5), pp. 1155–1159.
[169] Volz, S. G., and Chen, G., 1999, "Molecular Dynamics Simulation of Thermal Conductivity of Silicon Nanowires," Appl. Phys. Lett., **75**(14), pp. 2056–2058.
[170] He, Y. P., and Galli, G., 2012, "Microscopic Origin of the Reduced Thermal Conductivity of Silicon Nanowires," Phys. Rev. Lett., **108**(21), p. 215901.
[171] Donadio, D., and Galli, G., 2009, "Atomistic Simulations of Heat Transport in Silicon Nanowires," Phys. Rev. Lett., **102**(19), p. 195901.
[172] Chen, Y. F., Li, D. Y., Lukes, J. R., and Majumdar, A., 2005, "Monte Carlo Simulation of Silicon Nanowire Thermal Conductivity," ASME J. Heat Transfer, **127**(10), pp. 1129–1137.

[173] Tian, Z. T., Esfarjani, K., Shiomi, J., Henry, A. S., and Chen, G., 2011, "On the Importance of Optical Phonons to Thermal Conductivity in Nanostructures," Appl. Phys. Lett., **99**(5), p. 053122.
[174] Kazan, M., Guisbiers, G., Pereira, S., Correia, M. R., Masri, P., Bruyant, A., Volz, S., and Royer, P., 2010, "Thermal Conductivity of Silicon Bulk and Nanowires: Effects of Isotopic Composition, Phonon Confinement, and Surface Roughness," J. Appl. Phys., **107**(8), p. 083503.
[175] Mingo, N., 2003, "Calculation of Si Nanowire Thermal Conductivity Using Complete Phonon Dispersion Relations," Phys. Rev. B, **68**(11), p. 113308.
[176] Mingo, N., Yang, L., Li, D., and Majumdar, A., 2003, "Predicting the Thermal Conductivity of Si and Ge Nanowires," Nano Lett., **3**(12), pp. 1713–1716.
[177] Fuchs, K., 1938, "The Conductivity of Thin Metallic Films According to the Electron Theory of Metals," Proc. Cambridge Philos. Soc., **34**, pp. 100–108.
[178] Sondheimer, E. H., 1952, "The Mean Free Path of Electrons in Metals," Adv. Phys., **1**(1), pp. 1–42.
[179] Chen, R., Hochbaum, A. I., Murphy, P., Moore, J., Yang, P. D., and Majumdar, A., 2008, "Thermal Conductance of Thin Silicon Nanowires," Phys. Rev. Lett., **101**(10), p. 105501.
[180] Murphy, P. G., and Moore, J. E., 2007, "Coherent Phonon Scattering Effects on Thermal Transport in Thin Semiconductor Nanowires," Phys. Rev. B, **76**(15), p. 155313.
[181] Lim, J. W., Hippalgaonkar, K., Andrews, S. C., Majumdar, A., and Yang, P. D., 2012, "Quantifying Surface Roughness Effects on Phonon Transport in Silicon Nanowires," Nano Lett., **12**(5), pp. 2475–2482.
[182] Slack, G. A., 1979, "The Thermal Conductivity of Nonmetallc Crystals," *Solid State Physics*, H. Ehrenreich, F. Seitz, and D. Turnbull, eds., Academic Press, New York, pp. 1–73.
[183] Cahill, D. G., Watson, S. K., and Pohl, R. O., 1992, "Lower Limit to the Thermal Conductivity of Disordered Crystals," Phys. Rev. B, **46**(10), pp. 6131–6140.
[184] Chiritescu, C., Cahill, D. G., Nguyen, N., Johnson, D., Bodapati, A., Keblinski, P., and Zschack, P., 2007, "Ultralow Thermal Conductivity in Disordered, Layered WSe_2 Crystals," Science, **315**(5810), pp. 351–353.
[185] Costescu, R. M., Cahill, D. G., Fabreguette, F. H., Sechrist, Z. A., and George, S. M., 2004, "Ultra-Low Thermal Conductivity in W/Al_2O_3 Nanolaminates," Science, **303**(5660), pp. 989–990.
[186] Asheghi, M., Kurabayashi, K., Kasnavi, R., and Goodson, K. E., 2002, "Thermal Conduction in Doped Single-Crystal Silicon Films," J. Appl. Phys., **91**(8), pp. 5079–5088.
[187] Asheghi, M., Leung, Y. K., Wong, S. S., and Goodson, K. E., 1997, "Phonon-Boundary Scattering in Thin Silicon Layers," Appl. Phys. Lett., **71**(13), pp. 1798–1800.
[188] Uma, S., Mcconnell, A. D., Asheghi, M., Kurabayashi, K., and Goodson, K. E., 2001, "Temperature-Dependent Thermal Conductivity of Undoped Polycrystalline Silicon Layers," Int. J. Thermophys., **22**(2), pp. 605–616.
[189] Ju, Y. S., and Goodson, K. E., 1999, "Phonon Scattering in Silicon Films With Thickness of Order 100 nm," Appl. Phys. Lett., **74**(20), pp. 3005–3007.
[190] Cuffe, J., Chavez, E., Shchepetov, A., Chapuis, P. O., El Boudouti, E. H., Alzina, F., Kehoe, T., Gomis-Bresco, J., Dudek, D., Pennec, Y., Djafari-Rouhani, B., Prunnila, M., Ahopelto, J., and Torres, C. M. S., 2012, "Phonons in Slow Motion: Dispersion Relations in Ultrathin Si Membranes," Nano Lett., **12**(7), pp. 3569–3573.
[191] Cuffe, J., Chavez, E., Chapuis, P.-O., Alzina, F., Sotomayor Torres, C. M., Ristow, O., Hettich, M., Dekorsy, T., Shchepetov, A., Prunnila, M., and Ahopelto, J., 2013, "Lifetimes of Confined Acoustic Phonons in Ultrathin Silicon Membranes," Phys. Rev. Lett., **110**(9), p. 095503.
[192] Johnson, J. A., Maznev, A. A., Cuffe, J., Eliason, J. K., Minnich, A. J., Kehoe, T., Torres, C. M. S., Chen, G., and Nelson, K. A., 2013, "Direct Measurement of Room-Temperature Nondiffusive Thermal Transport Over Micron Distances in a Silicon Membrane," Phys. Rev. Lett., **110**(2), p. 025901.
[193] Chen, G., 1998, "Thermal Conductivity and Ballistic-Phonon Transport in the Cross-Plane Direction of Superlattices," Phys. Rev. B, **57**(23), pp. 14958–14973.
[194] Chen, G., 2002, "Ballistic-Diffusive Equations for Transient Heat Conduction From Nano to Macroscales," ASME J. Heat Transfer, **124**(2), pp. 320–328.
[195] Ren, S. Y., and Dow, J. D., 1982, "Thermal Conductivity of Superlattices," Phys. Rev. B, **25**(6), pp. 3750–3755.
[196] Colvard, C., Gant, T. A., Klein, M. V., Merlin, R., Fischer, R., Morkoc, H., and Gossard, A. C., 1985, "Folded Acoustic and Quantized Optic Phonons in (GaAl)As Superlattices," Phys. Rev. B, **31**(4), pp. 2080–2091.
[197] Hyldgaard, P., and Mahan, G. D., 1997, "Phonon Superlattice Transport," Phys. Rev. B, **56**(17), pp. 10754–10757.
[198] Chen, G., 1999, "Phonon Wave Heat Conduction in Thin Films and Superlattices," ASME J. Heat Transfer, **121**(4), pp. 945–953.
[199] Ward, A., and Broido, D. A., 2008, "Intrinsic Lattice Thermal Conductivity of Si/Ge and GaAs/AlAs Superlattices," Phys. Rev. B, **77**(24), p. 245328.
[200] Simkin, M. V., and Mahan, G. D., 2000, "Minimum Thermal Conductivity of Superlattices," Phys. Rev. Lett., **84**(5), pp. 927–930.
[201] Yang, B., and Chen, G., 2003, "Partially Coherent Phonon Heat Conduction in Superlattices," Phys. Rev. B, **67**(19), p. 195311.
[202] Daly, B. C., Maris, H. J., Imamura, K., and Tamura, S., 2002, "Molecular Dynamics Calculation of the Thermal Conductivity of Superlattices," Phys. Rev. B, **66**(2), p. 024301.
[203] Yu, J. K., Mitrovic, S., Tham, D., Varghese, J., and Heath, J. R., 2010, "Reduction of Thermal Conductivity in Phononic Nanomesh Structures," Nat. Nanotechnol., **5**(10), pp. 718–721.
[204] Luckyanova, M. N., Garg, J., Esfarjani, K., Jandl, A., Bulsara, M. T., Schmidt, A. J., Minnich, A. J., Chen, S., Dresselhaus, M. S., Ren, Z., Fitzgerald, E. A., and Chen, G., 2012, "Coherent Phonon Heat Conduction in Superlattices," Science, **338**(6109), pp. 936–939.
[205] Katika, K. M., and Pilon, L., 2008, "The Effect of Nanoparticles on the Thermal Conductivity of Crystalline Thin Films at Low Temperatures," J. Appl. Phys., **103**(11), p. 114308.
[206] Kim, W., and Majumdar, A., 2006, "Phonon Scattering Cross Section of Polydispersed Spherical Nanoparticles," J. Appl. Phys., **99**(8), p. 084306.
[207] McGaughey, A. J. H., and Jain, A., 2012, "Nanostructure Thermal Conductivity Prediction by Monte Carlo Sampling of Phonon Free Paths," Appl. Phys. Lett., **100**(6), p. 061911.
[208] Little, W. A., 1959, "The Transport of Heat Between Dissimilar Solids at Low Temperatures," Can. J. Phys., **37**(3), pp. 334–349.
[209] Swartz, E., and Pohl, R., 1989, "Thermal Boundary Resistance," Rev. Mod. Phys., **61**(3), pp. 605–668.
[210] Schelling, P., Phillpot, S., and Keblinski, P., 2002, "Phonon Wave-Packet Dynamics at Semiconductor Interfaces by Molecular-Dynamics Simulation," Appl. Phys. Lett., **80**(14), pp. 2484–2486.
[211] Sun, L., and Murthy, J., 2010, "Molecular Dynamics Simulation of Phonon Scattering at Silicon/Germanium Interfaces," ASME J. Heat Transfer, **132**(10), p. 102403.
[212] Zuckerman, N., and Lukes, J., 2008, "Acoustic Phonon Scattering From Particles Embedded in an Anisotropic Medium: A Molecular Dynamics Study," Phys. Rev. B, **77**(9), p. 094302.
[213] Tian, Z. T., White, B. E., and Sun, Y., 2010, "Phonon Wave-Packet Interference and Phonon Tunneling Based Energy Transport Across Nanostructured Thin Films," Appl. Phys. Lett., **96**(26), p. 263113.
[214] Young, D., and Maris, H., 1989, "Lattice Dynamics Calculation of the Kapitza Resistance Between FCC Lattices," Phys. Rev. B, **40**(6), pp. 3685–3693.
[215] Pettersson, S., and Mahan, G., 1990, "Theory of the Thermal Boundary Resistance Between Dissimilar Lattices," Phys. Rev. B, **42**(12), pp. 7386–7390.
[216] Zhao, H., and Freund, J., 2005, "Lattice-Dynamical Calculation of Phonon Scattering at Ideal Si-Ge Interfaces," J. Appl. Phys., **97**(2), p. 024903.
[217] Wang, J., and Wang, J., 2006, "Mode-Dependent Energy Transmission Across Nanotube Junctions Calculated With a Lattice Dynamics Approach," Phys. Rev. B, **74**(5), p. 054303.
[218] Zhang, W., Fisher, T., and Mingo, N., 2007, "The Atomistic Green's Function Method: An Efficient Simulation Approach for Nanoscale Phonon Transport," Numer. Heat Transfer, Part B, **51**(4), pp. 333–349.
[219] Volz, S., ed., 2009, *Thermal Nanosystems and Nanomaterials*, Vol. 118, Springer, Heidelberg, Germany, pp. 1–587.
[220] Zhang, W., Fisher, T., and Mingo, N., 2007, "Simulation of Interfacial Phonon Transport in Si-Ge Heterostructures Using an Atomistic Green's Function Method," ASME J. Heat Transfer, **129**(4), pp. 483–491.
[221] Hopkins, P., Norris, P., Tsegaye, M., and Ghosh, A., 2009, "Extracting Phonon Thermal Conductance Across Atomic Junctions: Nonequilibrium Green's Function Approach Compared to Semiclassical Methods," J. Appl. Phys., **106**(6), p. 063503.
[222] Li, X., and Yang, R., 2012, "Size-Dependent Phonon Transmission Across Dissimilar Material Interfaces," J. Phys.: Condens. Matter, **24**(15), p. 155302.
[223] Mingo, N., Stewart, D., Broido, D., and Srivastava, D., 2008, "Phonon Transmission Through Defects in Carbon Nanotubes From First Principles," Phys. Rev. B, **77**(3), p. 033418.
[224] Stewart, D., Savic, I., and Mingo, N., 2009, "First-Principles Calculation of the Isotope Effect on Boron Nitride Nanotube Thermal Conductivity," Nano Lett., **9**(1), pp. 81–84.
[225] Tian, Z. T., Esfarjani, K., and Chen, G., 2012, "Enhancing Phonon Transmission Across a Si/Ge Interface by Atomic Roughness: First-Principles Study With the Green's Function Method," Phys. Rev. B, **86**(23), p. 235304.
[226] Zhao, H., and Freund, J., 2009, "Phonon Scattering at a Rough Interface Between Two FCC Lattices," J. Appl. Phys., **105**(1), p. 013515.
[227] Nan, C. W., Birringer, R., Clarke, D. R., and Gleiter, H., 1997, "Effective Thermal Conductivity of Particulate Composites With Interfacial Thermal Resistance," J. Appl. Phys., **81**(10), pp. 6692–6699.
[228] Minnich, A., and Chen, G., 2007, "Modified Effective Medium Formulation for the Thermal Conductivity of Nanocomposites," Appl. Phys. Lett., **91**(7), p. 073105.
[229] Ordonez-Miranda, J., Yang, R. G., and Alvarado-Gil, J. J., 2011, "On the Thermal Conductivity of Particulate Nanocomposites," Appl. Phys. Lett., **98**(23), p. 233111.
[230] Maiti, A., Mahan, G. D., and Pantelides, S. T., 1997, "Dynamical Simulations of Nonequilibrium Processes—Heat Flow and the Kapitza Resistance Across Grain Boundaries," Solid State Commun., **102**(7), pp. 517–521.
[231] Schelling, P. K., Phillpot, S. R., and Keblinski, P., 2004, "Kapitza Conductance and Phonon Scattering at Grain Boundaries by Simulation," J. Appl. Phys., **95**(11), pp. 6082–6091.
[232] Chalopin, Y., Esfarjani, K., Henry, A., Volz, S., and Chen, G., 2012, "Thermal Interface Conductance in Si/Ge Superlattices by Equilibrium Molecular Dynamics," Phys. Rev. B, **85**(19), p. 195302.
[233] Tian, Z. T., 2009, "Nanoscale Heat Transfer in Argon-Like Solids via Molecular Dynamics Simulations," Ph.D. thesis, State University of New York at Binghamton, Binghamton, NY.
[234] Roberts, N. A., Walker, D. G., and Li, D. Y., 2009, "Molecular Dynamics Simulation of Thermal Conductivity of Nanocrystalline Composite Films," Int. J. Heat Mass Transfer, **52**(7–8), pp. 2002–2008.

[235] Tian, Z. T., Kim, S., Sun, Y., and White, B., 2009, "A Molecular Dynamics Study of Thermal Conductivity in Nanocomposites via the Phonon Wave Packet Method," Proceedings of the ASME InterPACK Conference 2009, Vol. 1, pp. 607–615.
[236] Prasher, R., 2006, "Thermal Conductivity of Composites of Aligned Nanoscale and Microscale Wires and Pores," J. Appl. Phys., **100**(3), p. 034307.
[237] Jeng, M.-S., Yang, R., Song, D., and Chen, G., 2008, "Modeling the Thermal Conductivity and Phonon Transport in Nanoparticle Composites Using Monte Carlo Simulation," ASME J. Heat Transfer, **130**(4), p. 042410.
[238] Peraud, J.-P. M., and Hadjiconstantinou, N. G., 2011, "Efficient Simulation of Multidimensional Phonon Transport Using Energy-Based Variance-Reduced Monte Carlo Formulations," Phys. Rev. B, **84**(20), p. 205331.
[239] Péraud, J.-P. M., and Hadjiconstantinou, N. G., 2012, "An Alternative Approach to Efficient Simulation of Micro/Nanoscale Phonon Transport," Appl. Phys. Lett., **101**(15), p. 153114.
[240] Schmidt, A. J., Collins, K. C., Minnich, A. J., and Chen, G., 2010, "Thermal Conductance and Phonon Transmissivity of Metal-Graphite Interfaces," J. Appl. Phys., **107**(10), p. 104907.
[241] Prasher, R., 2009, "Acoustic Mismatch Model for Thermal Contact Resistance of van der Waals Contacts," Appl. Phys. Lett., **94**(4), p. 041905.
[242] Min, G., and Rowe, D., 2000, "Improved Model for Calculating the Coefficient of Performance of a Peltier Module," Energy Convers. Manage., **41**(2), pp. 163–171.
[243] Chowdhury, I., Prasher, R., Lofgreen, K., Chrysler, G., Narasimhan, S., Mahajan, R., Koester, D., Alley, R., and Venkatasubramanian, R., 2009, "On-Chip Cooling by Superlattice-Based Thin-Film Thermoelectrics," Nat. Nanotechnol., **4**(4), pp. 235–238.
[244] Hatzikraniotis, E., Zorbas, K., Samaras, I., Kyratsi, T., and Paraskevopoulos, K., 2010, "Efficiency Study of a Commercial Thermoelectric Power Generator (TEG) Under Thermal Cycling," J. Electron. Mater., **39**(9), pp. 2112–2116.
[245] Barako, M. T., Park, W., Marconnet, A. M., Asheghi, M., and Goodson, K. E., 2012, "A Reliability Study With Infrared Imaging of Thermoelectric Modules Under Thermal Cycling," Proceedings of the IEEE Intersociety Conference on Thermal and Thermomechanical Phenomena in Electronic Systems (ITherm), San Diego, CA, pp. 86–92.
[246] Kashi, S., Keshavarz, M., Vasilevskiy, D., Masut, R., and Turenne, S., 2012, "Effect of Surface Preparation on Mechanical Properties of Ni Contacts on Polycrystalline $(Bi_{1-x}Sb_x)_2(Te_{1-y}Se_y)_3$ Alloys," J. Electron. Mater., pp. 1227–1231.
[247] Feng, H.-P., Yu, B., Chen, S., Collins, K., He, C., Ren, Z. F., and Chen, G., 2011, "Studies on Surface Preparation and Smoothness of Nanostructured Bi_2Te_3-Based Alloys by Electrochemical and Mechanical Methods," Electrochim. Acta, **56**(8), pp. 3079–3084.
[248] Gao, Y., Marconnet, A., Panzer, M., Leblanc, S., Dogbe, S., Ezzahri, Y., Shakouri, A., and Goodson, K., 2010, "Nanostructured Interfaces for Thermoelectrics," J. Electron. Mater., **39**(9), pp. 1456–1462.
[249] Mishra, H., Cola, B. A., Rawat, V., Amama, P. B., Biswas, K. G., Xu, X., Fisher, T. S., and Sands, T. D., 2009, "Thermomechanical and Thermal Contact Characteristics of Bismuth Telluride Films Electrodeposited on Carbon Nanotube Arrays," Adv. Mater., **21**(42), pp. 4280–4283.
[250] Yazawa, K., and Shakouri, A., 2011, "Cost-Efficiency Trade-Off and the Design of Thermoelectric Power Generators," Environ. Sci. Technol., **45**(17), pp. 7548–7553.
[251] Kraemer, D., Poudel, B., Feng, H.-P., Caylor, J. C., Yu, B., Yan, X., Ma, Y., Wang, X., Wang, D., Muto, A., McEnaney, K., Chiesa, M., Ren, Z., and Chen, G., 2011, "High-Performance Flat-Panel Solar Thermoelectric Generators With High Thermal Concentration," Nature Mater., **10**(7), pp. 532–538.
[252] Kraemer, D., McEnaney, K., Chiesa, M., and Chen, G., 2012, "Modeling and Optimization of Solar Thermoelectric Generators for Terrestrial Applications," Sol. Energy, **86**(5), pp. 1338–1350.